THE EUROPEAN
PHYSICAL JOURNAL C

CrossMark

Observers in Kerr spacetimes: the ergoregion on the equatorial plane

D. Pugliese[1,a], **H. Quevedo**[2,3,4]

[1] Faculty of Philosophy and Science, Institute of Physics, Silesian University in Opava, Bezručovo náměstí 13, 74601 Opava, Czech Republic
[2] Dipartimento di Fisica, Università di Roma "La Sapienza", 00185 Rome, Italy
[3] Instituto de Ciencias Nucleares, Universidad Nacional Autónoma de México, AP 70543, 04510 Mexico, DF, Mexico
[4] Department of Theoretical and Nuclear Physics, Kazakh National University, Almaty 050040, Kazakhstan

Abstract We perform a detailed analysis of the properties of stationary observers located on the equatorial plane of the ergosphere in a Kerr spacetime, including light-surfaces. This study highlights crucial differences between black hole and the super-spinner sources. In the case of Kerr naked singularities, the results allow us to distinguish between "weak" and "strong " singularities, corresponding to spin values close to or distant from the limiting case of extreme black holes, respectively. We derive important limiting angular frequencies for naked singularities. We especially study very weak singularities as resulting from the spin variation of black holes. We also explore the main properties of zero angular momentum observers for different classes of black hole and naked singularity spacetimes.

1 Introduction

The physics of black holes (**BHs**) is probably one of the most complex and still controversial aspects of Einstein's geometric theory of gravitation. Many processes of High Energy Astrophysics are supposed to involve singularities and their formation from a stellar progenitor collapse or from the merging of a binary **BH** system. The interaction of these sources with the matter environment, which can lead to accretion and jets emission, is the basis for many observed phenomena. As a consequence of this interaction, the singularity properties, determined generally by the values of their intrinsic spin, mass or electric charge parameters, might be modified, leading to considerable changes of the singularity itself. In this work, we concentrate our analysis on the ergoregion in the naked singularity (**NS**) and **BH** regimes of the axisymmetric and stationary Kerr solution. We are concerned also about

the implications of any spin-mass ratio oscillation between the **BH** and the **NS** regimes from the viewpoint of stationary observers and their frequencies, assuming the invariance of the system symmetries (axial symmetry and time independence). One of the goals of this work is to explore the existence of spin transitions in very weak naked singularities [2], which are characterized by a spin parameter $a/M \approx 1$. If the collapse of a stellar object or the merging of several stellar or **BH** attractors lead to the formation of a naked singularity, then a total or partial destruction of the horizon may occur which should be accompanied by oscillations of the spin-to-mass ratio. Naked singularities can also appear in non-isolated **BH** configurations as the result of their interaction with the surrounding matter, i. e., in some transient process of the evolution of an interacting black hole. Indeed, the interaction can lead to modifications of characteristic **BH** parameters, for instance, through a spin-up or spin-down process which can also alter the spacetime symmetries. The details of such spin transitions, leading possibly to the destruction of the horizon, and their consequences are still an open problem.

In this work, keeping the Kerr spacetime symmetries unchanged, we focus on the variation of the dimensionless spin parameter in the region within the static limit on the equatorial plane of the attractor, this being the plane of symmetry of the Kerr solution. This special plane of the axisymmetric geometry has many interesting properties; for instance, constants of motion emerge due to the symmetry under reflection with respect to this plane; the geometry has some peculiarities that make it immediately comparable with the limiting static Schwarzschild solution, in particular, the location of the outer ergoregion boundary is independent of the spin value, and coincides with the location of the Schwarzschild horizon. There is also a clear astrophysical interest in the exploration of such a plane, as the large

[a] e-mail: d.pugliese.physics@gmail.com

Springer

majority of accretion disks are considered to be located on the equatorial plane of their attractors.

From a methodological viewpoint, our analysis represents a comparative study of stationary and static observers in Kerr spacetimes for any range of the spin parameter. The findings in this work highlight major differences between the behavior of these observers in **BH** and **NS** geometries. These issues are clearly related to the most general and widely discussed problem of defining **BHs**, their event horizon and their intrinsic thermodynamic properties [3–8]. Further, it seems compelling to clarify the role of the static limit and of the ergoregion in some of the well-analyzed astrophysical processes such as the singularity formation, through the gravitational collapse of a stellar "progenitor" or the merging of two **BHs**. Similarly, it is interesting to analyze the role of the frame-dragging effect in driving the accretion processes. In fact, the ergosphere plays an important role in the energetics of rotating black holes.

The dynamics inside the ergoregion is relevant in Astrophysics for possible observational effects, since in this region the Hawking radiation can be analyzed and the Penrose energy extraction process occurs [9–13].[1] For the actual state of the Penrose process, see [15]. Another interesting effect connected directly to the ergoregion is discussed in [16]. The mechanism, by which energy from compact spinning objects is extracted, is of great astrophysical interest and the effects occurring inside the ergoregion of black holes are essential for understanding the central engine mechanism of these processes [17,18]. Accreting matter can even get out, giving rise, for example, to jets of matter or radiation [17,19] originated inside the ergoregion. Another possibility is the extraction of energy from a rotating black hole through the Blandford–Znajek mechanism (see, for instance, [20–29]). An interesting alternative scenario for the role of the Blandford–Znajek process in the acceleration of jets is presented in [30]. Further discussions on the Penrose and Blandford–Znajek processes may be found in [31,32]. In general, using orbits entering the ergosphere, energy can be extracted from a Kerr black hole or a naked singularity. On the other hand, naked singularity solutions have been studied in different contexts in

[33–42,44,45]. Kerr naked singularities as particle accelerators are considered in [43] – see also [44,45]. More generally, Kerr naked singularities can be relevant in connection to superspinars, as discussed in [44]. The stability of Kerr superspinars has been analyzed quite recently in [46], asserting the importance of boundary conditions in dealing with perturbations of **NSs**.

An interesting perspective exploring duality between elementary particles and black holes, pursuing quantum black holes as the link between microphysics and macrophysics, can be found in [47–50] – see also [51]. A general discussion on the similarities between characteristic parameter values of **BHs** and **NSs**, in comparison with particle like objects, is addressed also in [52–55]. Quantum evaporation of **NSs** was analyzed in [56], radiation in [57], and gravitational radiation in [58–60].

Creation and stability of naked singularities are still intensively debated [61–66]. A discussion on the ergoregion stability can be found in [67,68]. However, under quite general conditions on the progenitor, these analysis do not exclude the possibility that considering instability processes a naked singularity can be produced as the result of a gravitational collapse. These studies, based upon a numerical integration of the corresponding field equations, often consider the stability of the progenitor models and investigate the gravitational collapse of differentially rotating neutron stars in full general relativity [69]. Black hole formation is then associated with the formation of trapped surfaces. As a consequence of this, a singularity without trapped surfaces, as the result of a numerical integration, is usually considered as a proof of its naked singularity nature. However, the non existence of trapped surfaces after or during the gravitational collapse is not in general a proof of the existence of a naked singularity. As shown in [70], in fact, it is possible to choose a very particular slicing of spacetime during the formation of a spherically symmetric black hole where no trapped surfaces exist (see also [71]). Eventually, the process of gravitational collapse towards the formation of **BHs** (and therefore, more generally, the issues concerning the formation or not of a horizon and hence of **NSs**) is still, in spite of several studies, an open problem. There are transition periods of transient dynamics, possibly involving topological deformations of the spacetime, in which we know the past and future asymptotic regions of the spacetime, but it is still in fact largely unclear what happens during that process. The problem is wide and involves many factors as, especially in non-isolated systems, the role of matter and symmetries during collapse. Another major process that leads to black hole formation is the merging of two (or more) black holes, recently detected for the first time in the gravitational waves sector [72]. See also [73,74] for the first observation of the probable formation of a **BH** from the coalescence of two neutron stars. An interesting and detailed analysis of Kerr and Kerr–Newman naked singular-

---

[1] The Hawking process is essentially due to the vacuum fluctuation happening in the regions close to the **BH** horizon; it is not related to the properties of the ergoregion itself. The Hawking radiation is the (spontaneous) emission of thermal radiation which is created in the vacuum regions surrounding a **BH**, and leads to a decrease of the mass. Connected in many ways to the Unruh effects, it generally leads to the production of pairs of particles, one escaping to infinity while the other is trapped by the **BH** horizon. On the other hand, the Penrose energy extraction, or its wave-analogue of super-radiance, is related essentially to a classical (i.e. non quantum) phenomenon occurring in the ergoregion, $]r_+, r_\varepsilon^+[$, due to the frame-dragging of the spinning spacetime. In this way, energy can be extracted from the source, lowering its angular momentum. For a study of the Hawking radiation in Kerr and Kerr–Newman spacetimes see also [14].

ities in the broader context of braneworld Kerr–Newman (**B-KN**) spacetimes can be found in [75], where a new kind of instability, called mining instability, of some **B-KN** naked singularity spacetimes was found. In there, the exploration of the "causality violation region" is also faced. This is the region where the angular coordinate becomes timelike, leading eventually to closed timelike curves. Details on the relation between this region and the Kerr ergoregion can be found in the aforementioned reference.

In [2,52–55,76], we focused on the study of axisymmetric gravitational fields, exploring different aspects of spacetimes with **NSs** and **BHs**. The results of this analysis show a clear difference between naked singularities and black holes from the point of view of the stability properties of circular orbits.[2] This fact would have significant consequences for the extended matter surrounding the central source and, hence, in all processes associated with energy extraction. Indeed, imagine an accretion disk made of test particles which are moving along circular orbits on the equatorial plane of a Kerr spacetime. It turns out that in the case of a black hole the accretion disk is continuous whereas in the case of a naked singularity it is discontinuous. This means that we can determine the values of intrinsic physical parameters of the central attractor by analyzing the geometric and topological properties of the corresponding Keplerian accretion disk. In addition, these disconnected regions, in the case of a naked singularities, are a consequence of the repulsive gravity properties found also in many other black hole solutions and in some extensions or modifications of Einstein's theory. The effects of repulsive gravity in the case of the Kerr geometry were considered in [80] and [81]. Analogies between the effects of repulsive gravity and the presence of a cosmological constant was shown also to occur in regular black hole spacetimes or in strong gravity objects without horizons [82,83].

Several studies have already shown that it is necessary to distinguish between weak ($a/M \approx 1$) and strong naked singularities ($a/M >> 1$). It is also possible to introduce a similar classification for black holes; however, we prove here that only in the case of naked singularities there are obvious fundamental distinctions between these classes which are not present among the different black hole classes. Our focus is on strong **BHs**, and weak and very weak **NSs**. This analysis confirms the distinction between strong and weak **NSs** and **BHs**, characterized by peculiar limiting values for the spin parameters. Nevertheless, the existence and meaning of such limits is still largely unclear, and more investigation is due.

----

[2] Test particle motion can be used to determine the topological properties of general relativistic spacetimes [77–79]. Moreover, we proved that in certain **NS** geometries different regions of stable timelike circular orbits are separated from each other by empty regions; this means that an accretion disk made of test particles will show a particular ring-like structure with specific topological properties.

However, there are indications about the existence of such limits in different geometries, where weak and strong singularities could appear. In [2,52–55], it was established that the motion of test particles on the equatorial plane of black hole spacetimes can be used to derive information about the structure of the central source of gravitation; moreover, typical effects of repulsive gravity were observed in the naked singularity ergoregion (see also [34,84–86]). In addition, it was pointed out that there exists a dramatic difference between black holes and naked singularities with respect to the zero and negative energy states in circular orbits (stable circular geodesics with negative energy were for the first time discussed in [87]). The static limit would act indeed as a semi-permeable membrane separating the spacetime region, filled with negative energy particles, from the external one, filled with positive energy particles, gathered from infinity or expelled from the ergoregion with impoverishment of the source energy. The membrane is selective because it acts so as to filter the material in transient between the inner region and outside the static limit. This membrane wraps and selectively isolates the horizon in Kerr black holes and the singularity in superspinning solutions, partially isolating it from the outer region by letting selectively rotating infalling or outgoing matter to cross the static limit. As mentioned above, the ergoregion is involved in the **BH** spin-up and spin-down processes leading to a radical change of the dynamical structure of the region closest to the source and, therefore, potentially could give rise to detectable effects. It is possible that, during the evolutionary phases of the rotating object interacting with the orbiting matter, there can be some evolutionary stages of spin adjustment, for example, in the proximity of the extreme value ($a \lesssim M$) where the speculated spin-down of the **BH** can occur preventing the formation of a naked singularity with $a \gtrsim M$ (see also [40,63,65,88–95]). The study of extended matter configurations in the Kerr ergoregion is faced for example in [2,96]. In [96–100], a model of multi-accretion disks, so called ringed accretion disks, both corotating and counterrotating on the equatorial plane of a Kerr **BH**, has been proposed, and a model for such ringed accretion disks was developed. Matter can eventually be captured by the accretion disk, increasing or removing part of its energy and angular momentum, therefore prompting a shift of its spin [64,87,101–104]. A further remarkable aspect of this region is that the outer boundary on the equatorial plane of the central singularity is invariant for every spin change, and coincides with the radius of the horizon of the static case. In the limit of zero rotation, the outer ergosurface coalesces with the event horizon. The extension of this region increases with the spin-to-mass ratio, but the outer limit is invariant. Although on the equatorial plane the ergoregion is invariant with respect to any transformation involving a change in the source spin (but not with respect to a change in the mass M), the dynamical structure of the ergoregion

is not invariant with respect to a change in the spin-to-mass ratio. Nevertheless, concerning the invariance of this region with respect to spin shifts it has been argued, for example in [105], that the ergoregion cannot indeed disappear as a consequence of a change in spin, because it may be filled by negative energy matter provided by the emergence of a Penrose process[3] [13]. The presence of negative energy particles, a distinctive feature of the ergoregion of any spinning source in any range of the spin value, has special properties when it comes to the circular motion in weakly rotating naked singularities. The presence of this special matter in an "antigravity" sphere, possibly filled with negative energy formed according to the Penrose process, and bounded by orbits with zero angular momentum, is expected to play an important role in the source evolution. In this work, we clarify and deepen those results, formulate in detail those considerations, analyze the static limit, and perform a detailed study of this region from the point of view of stationary observers. In this regards, we mention also the interesting and recent results published in [106] and [107].

In detail, this article is organized as follows: in Sect. 2 we discuss the main properties of the Kerr solution and the features of the ergoregion in the equatorial plane of the Kerr spacetimes. Concepts and notation used throughout this work are also introduced. Stationary observers in **BH** and **NS** geometries are introduced in Sect. 3. Then, in Sect. 4, we investigate the case of zero angular momentum observers and find all the spacetime configurations in which they can exist. Finally, in Sect. 5, we discuss our results.

2 Ergoregion properties in the Kerr spacetime

The Kerr metric is an axisymmetric, stationary (nonstatic), asymptotically flat exact solution of Einstein's equations in vacuum. In spheroidal-like Boyer–Lindquist (BL) coordinates, the line element can be written as

$$ds^2 = -dt^2 + \frac{\rho^2}{\Delta}dr^2 + \rho^2 d\theta^2 + (r^2 + a^2)\sin^2\theta d\phi^2$$
$$+ \frac{2M}{\rho^2}r(dt - a\sin^2\theta d\phi)^2, \qquad (1)$$

$$\Delta \equiv r^2 - 2Mr + a^2, \quad \text{and} \quad \rho^2 \equiv r^2 + a^2\cos^2\theta. \qquad (2)$$

The parameter $M \geq 0$ is interpreted as the mass parameter, while the rotation parameter $a \equiv J/M \geq 0$ (*spin*) is the *specific* angular momentum, and J is the *total* angular momentum of the gravitational source. The spherically symmetric (static) Schwarzschild solution is a limiting case for $a = 0$.

A Kerr black hole (**BH**) geometry is defined by the range of the spin-mass ratio $a/M \in]0, 1[$, the extreme black hole case corresponds to $a = M$, whereas a super-spinner Kerr compact object or a naked singularity (**NS**) geometry occurs when $a/M > 1$.

The Kerr solution has several symmetry properties. The Kerr metric tensor (1) is invariant under the application of any two different transformations: $\mathscr{P}_\mathbf{Q} : \mathbf{Q} \to -\mathbf{Q}$, where $\mathbf{Q}$ is one of the coordinates (t, ϕ) or the metric parameter a while a single transformation leads to a spacetime with an opposite rotation with respect to the unchanged metric. The metric element is independent of the coordinate t and the angular coordinate ϕ. The solution is stationary due to the presence of the Killing field $\xi_t = \partial_t$ and the geometry is axisymmetric as shown by the presence of the rotational Killing field $\xi_\phi = \partial_\phi$.

An observer orbiting, with uniform angular velocity, along the curves $r =$constant and $\theta =$constant will not see the spacetime changing during its motion. As a consequence of this, the covariant components p_ϕ and p_t of the particle four-momentum are conserved along the geodesics[4] and we can introduce the constants of motion

$$\mathscr{E} \equiv -g_{\alpha\beta}\xi_t^\alpha p^\beta, \quad \mathscr{L} \equiv g_{\alpha\beta}\xi_\phi^\alpha p^\beta. \qquad (3)$$

The constant of motion (along geodesics) $\mathscr{L}$ is interpreted as the angular momentum of the particle as measured by an observer at infinity, and we may interpret $\mathscr{E}$, for timelike geodesics, as the total energy of a test particle coming from radial infinity, as measured by a static observer located at infinity.

As a consequence of the metric tensor symmetry under reflection with respect to the equatorial hyperplane $\theta = \pi/2$, the equatorial (circular) trajectories are confined in the equatorial geodesic plane. Several remarkable surfaces characterize these geometries: for black hole and extreme black hole spacetimes the radii

$$r_\pm \equiv M \pm \sqrt{M^2 - a^2} : g^{rr} = 0 \qquad (4)$$

---

[3] We note that the wave analog of the Penrose process is the superradiant scattering.

[4] We adopt the geometrical units $c = 1 = G$ and the signature $(-, +, +, +)$, Greek indices run in $\{0, 1, 2, 3\}$. The four-velocity satisfy $u^\alpha u_\alpha = -1$. The radius r has units of mass $[M]$, and the angular momentum units of $[M]^2$, the velocities $[u^t] = [u^r] = 1$ and $[u^\phi] = [u^\theta] = [M]^{-1}$ with $[u^\phi/u^t] = [M]^{-1}$ and $[u_\phi/u_t] = [M]$. For the sake of convenience, we always consider a dimensionless energy and effective potential $[V_{eff}] = 1$ and an angular momentum per unit of mass $[L]/[M] = [M]$.

are the event outer and inner (Killing) horizons,[5] whereas

$$r_\varepsilon^\pm \equiv M \pm \sqrt{M^2 - a^2 \cos^2\theta} : g_{tt} = 0 \qquad (5)$$

are the outer and inner *ergosurfaces*, respectively,[6] with $r_\varepsilon^- \leq r_- \leq r_+ \leq r_\varepsilon^+$. In an extreme **BH** geometry, the horizons coincide, $r_- = r_+ = M$, and the relation $r_\varepsilon^\pm = r_\pm$ is valid on the rotational axis (i.e., when $\cos^2\theta = 1$).

In this work, we will deal particularly with the geometric properties of the *ergoregion* $\Sigma_\varepsilon^+ :]r_+, r_\varepsilon^+]$; in this region, we have that $g_{tt} > 0$ on the *equatorial plane* ($\theta = \pi/2$) and also $r_\varepsilon^+\big|_{\pi/2} = r_+\big|_{a=0} = 2M$ and $r_\varepsilon^- = 0$. The outer boundary r_ε^+ is known as the *static* (or also stationary) limit [108]; it is a *timelike* surface except on the axis of the Kerr source where it matches the outer horizon and becomes null-like. On the equatorial plane of symmetry, $\rho = r$ and the spacetime singularity is located at $r = 0$. In the naked singularity case, where the singularity at $\rho = 0$ is not covered by a horizon, the region Σ_ε^+ has a toroidal topology centered on the axis with the inner circle located on the singularity. On the equatorial plane, as $a \to 0$ the geometry "smoothly" resembles the spherical symmetric case, $r_+ \equiv r_\varepsilon^+\big|_{\pi/2}$, and the frequency of the signals emitted by an infalling particle in motion towards $r = 2M$, as seen by an observer at infinity, goes to zero.

In general, for $a \neq 0$ and $r \in \Sigma_\varepsilon^+$, the metric component g_{tt} changes its sign and vanishes for $r = r_\varepsilon^+$ (and $\cos^2\theta \in]0, 1]$). In the ergoregion, the Killing vector $\xi_t^\alpha = (1, 0, 0, 0)$ becomes spacelike, i.e., $g_{\alpha\beta}\xi_t^\alpha\xi_t^\beta = g_{tt} > 0$. As the quantity $\mathscr{E}$, introduced in Eq. (3), is associated to the Killing field $\xi_t = \partial_t$, then the particle energy can be also negative inside Σ_ε^+. For stationary spacetimes ($a \neq 0$) in Σ_ε^+, the motion with $\phi = const$ is *not* possible and all particles are forced to rotate with the source, i.e., $\dot\phi a > 0$. This fact implies in particular

that an observer with four-velocity proportional to ξ_t^α so that $\dot\theta = \dot r = \dot\phi = 0$, (the dot denotes the derivative with respect to the proper time τ along the trajectory), cannot exist inside the ergoregion. Therefore, for any infalling matter (timelike or photonlike) approaching the horizon r_+ in the region Σ_ε^+, it holds that $t \to \infty$ and $\phi \to \infty$, implying that the worldlines around the horizon, as long as $a \neq 0$, are subjected to an infinite twisting. On the other hand, trajectories with $r = const$ and $\dot r > 0$ (particles crossing the static limit and escaping outside in the region $r \geq r_\varepsilon^+$) are possible.

Concerning the frequency of a signal emitted by a source in motion along the boundary of the ergoregion r_ε^+, it is clear that the proper time of the source particle is not null.[7] Then, for an observer at infinity, the particle will reach and penetrate the surface $r = r_\varepsilon^+$, in general, in a finite time t. For this reason, the ergoregion boundary is *not* a surface of infinite redshift, except for the axis of rotation where the ergoregion coincides with the event horizon [2,109]. This means that an observer at infinity will see a non-zero emission frequency. In the spherical symmetric case ($a = 0$), however, as $g_{t\phi} = 0$ the proper time interval $d\tau = \sqrt{|g_{tt}|}dt$ goes to zero as one approaches $r = r_+ = r_\varepsilon^+$. For a timelike particle with positive energy (as measured by an observer at infinity), it is possible to cross the static limit and to escape towards infinity. In Sect. 3, we introduce stationary observers in **BH** and **NS** geometries. We find the explicit expression for the angular velocity of stationary observers, and perform a detailed analysis of its behavior in terms of the radial distance to the source and of the angular momentum of the gravity source. We find all the conditions that must be satisfied for a light-surface to exist.

3 Stationary observers and light surfaces

We start our analysis by considering *stationary observers* which are defined as observers whose tangent vector is a spacetime Killing vector; their four-velocity is therefore a linear combination of the two Killing vectors ξ_ϕ and ξ_t, i.e., the coordinates r and θ are constants along the worldline of a stationary observer [110]. As a consequence of this property, a stationary observer does not see the spacetime changing along its trajectory. It is convenient to introduce the (uniform) *angular velocity* ω as

$$d\phi/dt = u^\phi/u^t \equiv \omega, \quad \text{or} \quad u^\alpha = \gamma(\xi_t^\alpha + \omega\xi_\phi^\alpha), \qquad (6)$$

which is a dimensionless quantity. Here, γ is a normalization factor

$$\gamma^{-2} \equiv -\kappa(\omega^2 g_{\phi\phi} + 2\omega g_{t\phi} + g_{tt}), \qquad (7)$$

---

[5] A Killing horizon is a *null* surface, $\mathscr{S}_0$, whose *null* generators coincide with the orbits of an one-parameter group of isometries (i. e., there is a Killing field $\mathscr{L}$ which is normal to $\mathscr{S}_0$). Therefore, it is a lightlike hypersurface (generated by the flow of a Killing vector) on which the norm of a Killing vector goes to zero. In static **BH** spacetimes, the event, apparent, and Killing horizons with respect to the Killing field ξ_t coincide. In the Schwarzschild spacetime, therefore, $r = 2M$ is the Killing horizon with *respect* to the Killing vector ∂_t. The event horizons of a spinning **BH** are Killing horizons with respect to the Killing field $\mathscr{L}_h = \partial_t + \omega_h\partial_\phi$, where ω_h is defined as the angular velocity of the horizon. In this article we shall extensively discuss this special vector in the case of **NS** geometries. We note here that the surface gravity of a **BH** may be defined as the rate at which the norm of the Killing vector vanishes from the outside. The surface gravity, $\mathscr{SG}_{Kerr} = (r_+ - r_-)/2(r_+^2 + a^2)$, is a conformal invariant of the metric, but it rescales with the conformal Killing vector. Therefore, it is not the same on all generators (but obviously it is constant along one specific generator because of the symmetries).

[6] In the Kerr solution, the Killing vector ∂_t, representing time translations at infinity, becomes null at the outer boundary of the ergoregion, r_ε^+, which is however a timelike surface; therefore, r_ε^+ is *not* a Killing horizon. More precisely, on the ergosurfaces the time translational Killing vector becomes null.

[7] However, since $g_{tt}(r_\varepsilon^\pm) = 0$, it is also known as an infinity redshift surface; see, for example, [108].

where $g_{\alpha\beta}u^{\alpha}u^{\beta} = -\kappa$. The particular case $\omega = 0$ defines *static observers*; these observers cannot exist in the ergoregion.

The angular velocity of a timelike stationary observer ($\kappa = +1$) is defined within the interval

$$\omega \in]\omega_-, \omega_+[\quad \text{where} \quad \omega_\pm \equiv \omega_Z \pm \sqrt{\omega_Z^2 - \omega_*^2},$$
$$\omega_*^2 \equiv \frac{g_{tt}}{g_{\phi\phi}} = \frac{g^{tt}}{g^{\phi\phi}}, \quad \omega_Z \equiv -\frac{g_{\phi t}}{g_{\phi\phi}}, \tag{8}$$

as illustrated in Figs. 1 and 2-*right*, where the frequencies $\omega_\pm$ are plotted for fixed values of r/M and as functions of the spacetime spin a/M and radius r/M, respectively. In particular, the combination

$$\mathscr{L}_\pm \equiv \xi_t + \omega_\pm \xi_\phi \tag{9}$$

defines null curves, $g_{\alpha\beta}\mathscr{L}_\pm^\alpha \mathscr{L}_\pm^\beta = 0$, and, therefore, as we shall see in detail below, the frequencies $\omega_\pm$ are limiting angular velocities for physical observers, defining a family of null curves, rotating with the velocity $\omega_\pm$ around the axis of symmetry. The Killing vectors $\mathscr{L}_\pm$ are also generators of Killing event horizons. The Killing vector $\xi_t + \omega\xi_\phi$ becomes
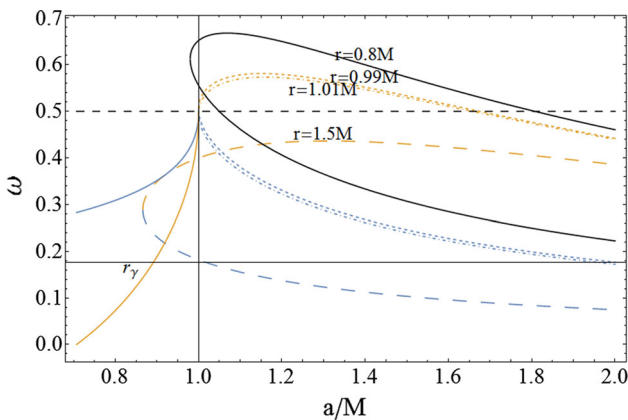

Fig. 1 Plot of the limit frequencies $\omega_\pm$ for fixed values of r/M. Frequencies $\omega_\pm$, on $r = r_\gamma \in \Sigma_\varepsilon^+$, photon circular orbit in the **BHs** ergoregion are also plotted – see Table 1 and [2]

null at r = r_+. At the horizon $\omega_+ = \omega_-$ and, consequently, stationary observers cannot exist inside this surface.

3.1 The frequencies $\omega_\pm$

We are concerned here with the orbits $r =$ const and $\omega =$ const, which are eligible for stationary observers. This analysis enlightens the differences between **NS** and **BH** spacetimes. Inside the ergoregion, the quantity in parenthesis in the r.h.s. of Eq. (7) is well defined for any source. However, it becomes null for photon-like particles and the rotational frequencies $\omega_\pm$. On the equatorial plane, the frequencies $\omega_\pm$ are given as

$$\omega_\pm \equiv \frac{2aM^2 \pm M\sqrt{r^2\Delta}}{r^3 + a^2(2M + r)}$$

with $\omega_\pm(r_+) = \omega_Z(r_+) = \omega_h \equiv \frac{a}{2r_+} \equiv \frac{M}{2\omega_0 r_+}$,

and $\lim_{r\to\infty} \omega_\pm = 0, \quad \lim_{r\to 0} \omega_\pm = \omega_0 \equiv \frac{M}{a}$. $\tag{10}$

Moreover, for the case of very strong naked singularities $a \gg M$, we obtain that $\omega_\pm \to 0$.

The above quantities are closely related to the main black hole characteristics, and determine also the main features that distinguish **NS** solutions from **BH** solutions. The constant ω_h plays a crucial role for the characterization of black holes, including their thermodynamic properties. It also determines the uniform (rigid) angular velocity on the horizon, representing the fact that the black hole rotates rigidly. This quantity enters directly into the definition of the **BH** surface gravity and, consequently, into the formulation of the rigidity theorem and into the expressions for the Killing vector (6). More precisely, the Kerr **BH** surface gravity is defined as $\kappa = \kappa_s - \gamma_a$, where $\kappa_s \equiv 1/4M$ is the Schwarzschild surface gravity, while $\gamma_a = M\omega_h^2$ (the effective spring constant, according to [111]) is the contribution due to the additional component of the **BH** intrinsic spin; ω_h is therefore the angular velocity (in units of $1/M$) on the *event horizon*. The (strong) rigidity theorem connects then the event horizon with a Killing horizon stating that, under suitable conditions,
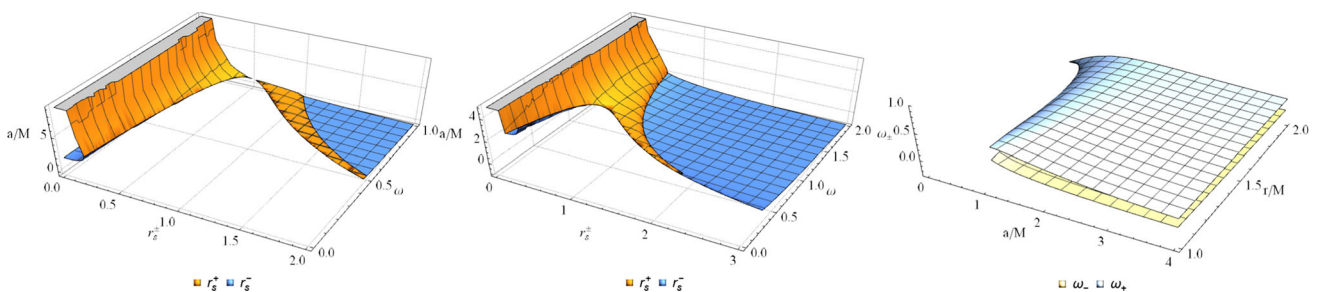

Fig. 2 Left and central panels: plot of the limit radii $r_s^\pm$ as functions of the spacetime spin a/M and frequencies ω – see also Fig. 4. Right panel: plot of the limit frequencies $\omega_\pm$ as functions of the spacetime spin a/M and radius r/M – see also Fig. 5

the event horizon of a stationary (asymptotically flat solution with matter satisfying suitable hyperbolic equations) **BH** is a Killing horizon.[8]

The constant limit $\omega_0 \equiv M/a$ plays an important role because it corresponds to the asymptotic limit for very small values of r and $R \equiv r/a$. Note that, on the equatorial plane, $g_{\alpha\beta}\mathscr{L}_0^\alpha \mathscr{L}_0^\beta = R^2$, where $\mathscr{L}_0 \equiv \mathscr{L}_\pm|_{\omega_0}$. The asymptotic behavior of these frequencies may be deeper investigated by considering the power series expansion for the spin parameter and the radius determined by the expression

$$\text{for } r \to \infty : \; \omega_\pm = \pm \frac{M}{r}\left(1 - \frac{M}{r}\right) + o[r^{-3}], \tag{11}$$

which shows a clear decreasing as the gravitational field diminishes. For large values of the rotational parameter, we obtain

$$\omega_\pm = \frac{M}{a}\frac{2M \pm r}{2M + r} + \frac{M}{a^3}\frac{r^2}{(2M+r)^2}$$
$$\times \left(\mp 2M^2 - 2Mr \mp \frac{1}{2}r^2\right) + o[a^{-5}], \tag{12}$$

so that for extreme large values of the source rotation, the frequencies vanish and no stationary observers exist, thought differently for the limiting frequencies $\omega_\pm$ (see Fig. 2). It is therefore convenient to introduce the dimensionless radius $R \equiv r/a$, for which we obtain the limit

$$R \to 0 : \; \omega_+ = \frac{M}{a} - \frac{MR^2}{2a} - \frac{M^2 R^3}{4a^2} + o[R^3]; \tag{13}$$

$$\omega_- = \frac{M}{a} - R + \frac{(M^2 + a^2)R^2}{2Ma}$$
$$- \frac{(a^4 + 4M^2 a^2 - M^4)R^3}{4a^2 M^2} + o[R^3]; \tag{14}$$

$$R \to \infty : \; \omega_\pm = \frac{(\mp M^2 + 4Ma \mp a^2)M}{2a^3 R^3}$$
$$\mp \frac{M^2}{a^2 R^2} \pm \frac{M}{aR} + o[R^{-3}]. \tag{15}$$

Equations (12), (13) and (14) show the particularly different behavior of $\omega_\pm$ with respect to the asymptote ω_0. The behavior of the frequencies for fixed values of the radial coordinate r and varying values of the specific rotational parameter a/M is illustrated in Fig. 1. We see that the region of allowed values for the frequencies is larger for naked singularities than for black holes. In fact, for certain values of the radial coordinate r, stationary observers can exist only in the field of naked singularities. This is a clear indication of the observational

differences between black holes and naked singularities. The allowed values for the frequencies are bounded by the limiting value $\omega_0 = M/a$; for a broader discussion on the role of the dimensionless spin parameter a/M in Kerr geometries, see also [96].[9] Moreover, for a given value of $\omega_\pm$, the corresponding radius is located at a certain distance from the source, depending on the value of the rotational parameter a. The following configuration of frequencies, radii and spin determines the location structure of stationary observers:

$$\omega_+ \in]0, \omega_0[, \; \text{for } a \in]0, M[\text{ in } r \in]0, r_-] \cup [r_+, +\infty[$$
$$\text{and for } a \geq M \text{ in } r > 0 \tag{16}$$
$$\omega_- \in]0, \omega_0[\; \text{for } a \in]0, M[\text{ in } r \in]0, r_-] \cup [r_+, r_\varepsilon^+[$$
$$\text{and for } a \geq M \text{ in } r \in]0, r_\varepsilon^+[. \tag{17}$$

Thus, we see that in the interval $]0, M/a[$ observers can exist with frequencies $\omega_\pm$; moreover, the frequency ω_- is allowed in $r \in \Sigma_\varepsilon^+$, while observers with $\omega_- < 0$ can exist in $r > r_\varepsilon^+$. Moreover, it is possible to show that, in **BH** geometries, the condition $\omega_\pm \ngtr 1/2$ must be satisfied outside the outer horizon ($r > r_+$). The particular value $\omega_\pm = \omega_h = 1/2$ is therefore the limiting angular velocity in the case of an extreme black hole, i.e., for $a = M$ so that $r = r_+ = r_- = M$ in Eq. (10). The behavior of the special frequency $\omega_\pm = 1/2$ is depicted in Fig. 3 and in Figs. 2, 4, 5, and 6, where other relevant frequencies are also plotted.

Equation (16) enlighten some important properties of the light surfaces (frequencies $\omega_\pm$) and of stationary observers, associated with frequencies $\omega \in]\omega_-, \omega_+[$ in the regime of strong singularities. Equation (16) also enlighten the dependence of the frequencies on the dimensionless spin a/M and radius $R = r/a$. It is clear that when the frequency interval $]\omega_-, \omega_+[$ shrinks, depending on the singularity spin a/M or the distance from the source r/M, the range of possible frequencies for stationary observers reduces. This occurs in general when $\omega_+ \approx \omega_-$. According to Eq. (16), the frequencies $\omega_\pm$ are bounded from above by the limiting frequencies $\omega_0 = M/a$ and from below by the null value $\omega_\pm = 0$. Thus, at fixed radius r, for very strong naked singularities $a/M \gg 1$, we have that $\omega_0 \approx 0$ and the range of possible frequencies for stationary observers becomes smaller. This effect will be discussed more deeply in Sect. 3.2, where we shall focus specifically on the frequency ω_0. On the other

---

[8] Assuming the cosmic censorship validity, the gravitational collapse should lead to **BH** configurations. The surface area of the **BH** event horizon is non-decreasing with time (which is the content of the second law of black hole thermodynamics). The **BH** event horizon of this stationary solution is a Killing horizon with constant surface gravity (zeroth law) [4,112–114].

[9] For simplicity we use here dimensionless quantities. We introduce the rotational version of the Killing vectors ξ_t and ξ_ϕ, i.e., the canonical vector fields $\tilde{V} \equiv (r^2 + a^2)\partial_t + a\partial_\phi$ and $\tilde{W} \equiv \partial_\phi + a\sigma^2 \partial_t$. Then, the contraction of the geodesic four-velocity with $\tilde{W}$ leads to the (non-conserved) quantity $\mathscr{L} - \mathscr{E}a\sigma^2$, which is a function of the conserved quantities $(\mathscr{E}, \mathscr{L})$, the spacetime parameter a and the polar coordinate θ; on the equatorial plane, it then reduces to $\mathscr{L} - \mathscr{E}a$. When we consider the principal null congruence $\gamma_\pm \equiv \pm\partial_r + \Delta^{-1}\tilde{V}$, the angular momentum $\mathscr{L} = a\sigma^2$, that is, $\bar{\ell} = 1$ (and $\mathscr{E} = +1$, in proper units), every principal null geodesic is then characterized by $\bar{\ell} = 1$. On the horizon, it is $\mathscr{L} = \mathscr{E} = 0$ [96,115].
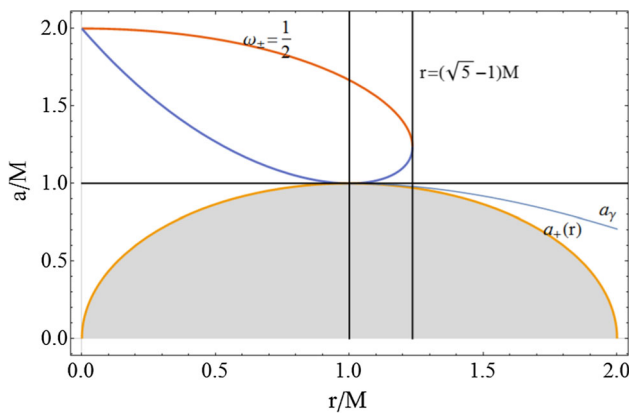
Fig. 3 Plot of the limiting frequency $\omega_\pm = 1/2$. The spin $a_+(r) \equiv \sqrt{r(2M-r)}$, solution of $r = r_+$, and a_γ, solution of $r = r_\gamma$ where $r_\gamma \in \Sigma_\varepsilon^+$ is the photon orbit in the ergoregion in a Kerr **BH**, are also plotted
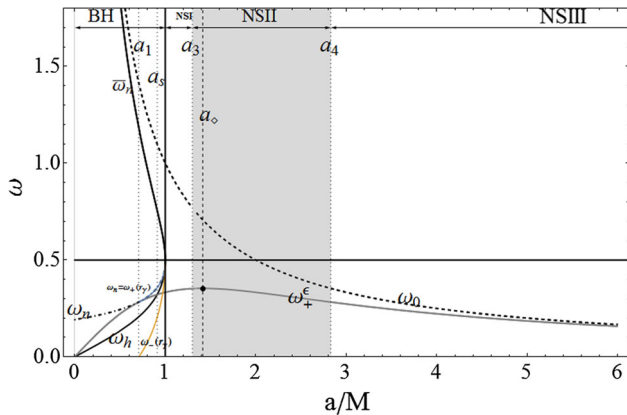

Fig. 4 Stationary observers: the angular velocities ω_+^ε (gray curve), ω_h (black curve), ω_n (dot-dashed curve), ω_0 (dashed curve), $\bar\omega_n > \omega_n > \omega_h$ (black thick curve). Here $\bar\omega_n = \omega_n = \omega_h = 1/2$ at $a = M$, $\omega_+^\varepsilon = \omega_h = 0.321797$ at $a = a_s$, and $\omega_+^\varepsilon = \omega_n = 0.282843$ at $a = a_1$. The maximum of ω_+^ε, at $a = a_\diamond = \sqrt{2}M$ (dashed line) where $a_\diamond : r_e = r_\varepsilon^+$ – see Eq. (31), is marked with a point. See also Fig. 2. The angular velocities $\omega_\pm$ on the **BH** photon orbit $r_\gamma \in \Sigma_\varepsilon^+$ are also plotted. Note that ω_n it is an extension of $\omega_+(r_\gamma)$ for $a < a_1$ – see Table 2

Fig. 5 Upper panel: plot of the curves $r_s^- =$constant and $r_s^+ =$constant (inside panel) in the plane $(\omega, a/M)$. The numbers denote the constant radii $r_s^\pm/M$ (light cylinders). Bottom panel: the radii $r_s^\pm$ versus the spin a/M, for different values of the velocity ω (numbers close to the curves), the gray region is $a \in [0, M]$ (**BH**-spacetime). The black region corresponds to $r < r_+$. The dashed lines denote $a_1 < a_2 < a_3 < a_4$. The angular momentum and the velocity (a, ω) for $r_s^\pm(a, \omega) = 0$ are related by $\omega = M/a$. See also Fig. 2

hand, considering the limits (10), together with Eqs. (11)–(15), we find that the range of possible frequencies shrinks also in the following situations: when moving outwardly with respect to the singularity (at fixed a), very close to the source, approaching the horizon r_h according to Eq. (10), or also for very large or very small $R = r/a$. The last case points out again the importance of the scaled radius r/a.

Essentially, stationary observers can be near the singularity only at a particular frequency. The greater is the **NS** dimensionless spin, the lower is the limiting frequency $\omega_\pm$, with the extreme limit at $\omega_+ = \omega_-$. In other words, the frequency range, $]\omega_-, \omega_+[$, for stationary observers vanishes as the value $r = 0$ is approached. The singularity at $r = 0$ in the **NS** regime is actually related to the characteristic constant
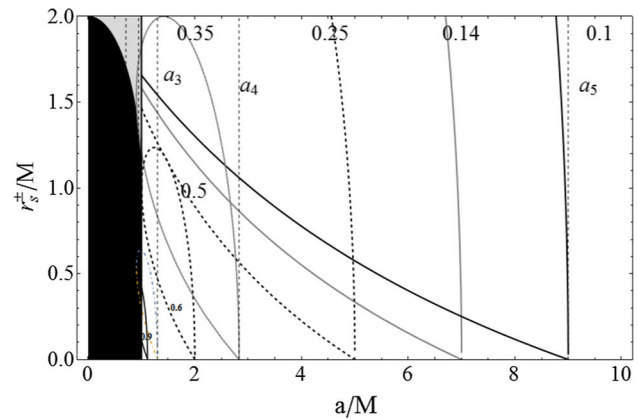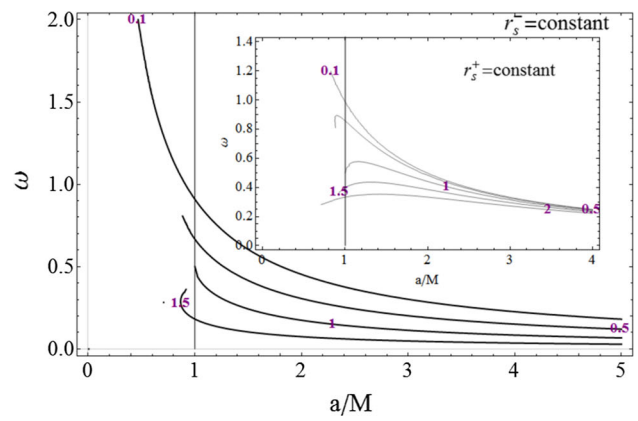
frequency $\omega = \omega_0$ in the same way as in **BH**-geometries the outer horizon $r = r_+$ is related to the constant frequency ω_h (cf. Eq. (10)). Consequently, a **NS** solution must be characterized by the frequency ω_0 and a **BH** solution by the frequency ω_h. Therefore, the frequency ω_0 may be seen actually as the **NS** counterpart of the **BH** horizon angular frequency ω_h (see Fig. 4). For $r > r_+$, it holds that $\omega_+ > \omega_-$.

Then, in general, for **BHs** and **NSs** in the static limit $r_\varepsilon^+ = 2M$, we obtain that

$$\omega_+^\varepsilon \equiv \omega_+(r_\varepsilon^+) = \frac{aM}{2M^2 + a^2} \quad \text{with} \quad \omega_-(r_\varepsilon^+) = 0. \quad (18)$$

Moreover, $\omega_- < 0$ for $r > r_\varepsilon^+$, and $\omega_- > 0$ inside the ergoregion Σ_ε^+, while $\omega_+ > 0$ everywhere.

In general, any frequency value should be contained within the range $\omega_+ - \omega_-$; therefore, it is convenient to define the *frequency interval*

$$\Delta_{\omega_\pm} \equiv \omega_+ - \omega_- = 2\sqrt{\omega_Z^2 - \omega_*^2}, \quad (19)$$
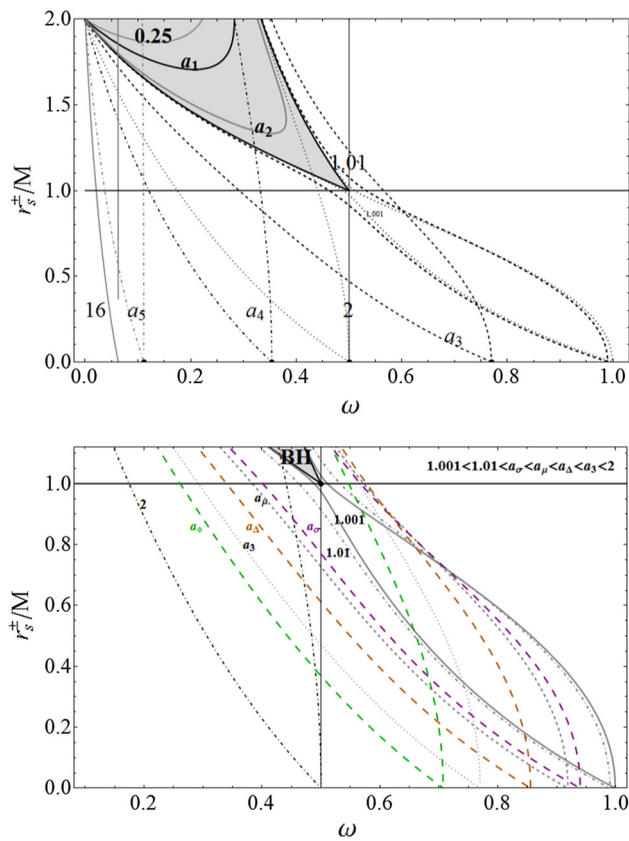
Fig. 6 The radii $r_s^\pm$ versus the frequency ω for different values of the spin a/M (numbers close to the curves). The gray region is the only region allowed for the case of **BH** spacetimes. The surfaces $\hat{r}_\pm$ at $a = M$ (extreme-**BH**-case) are shown in black-thick
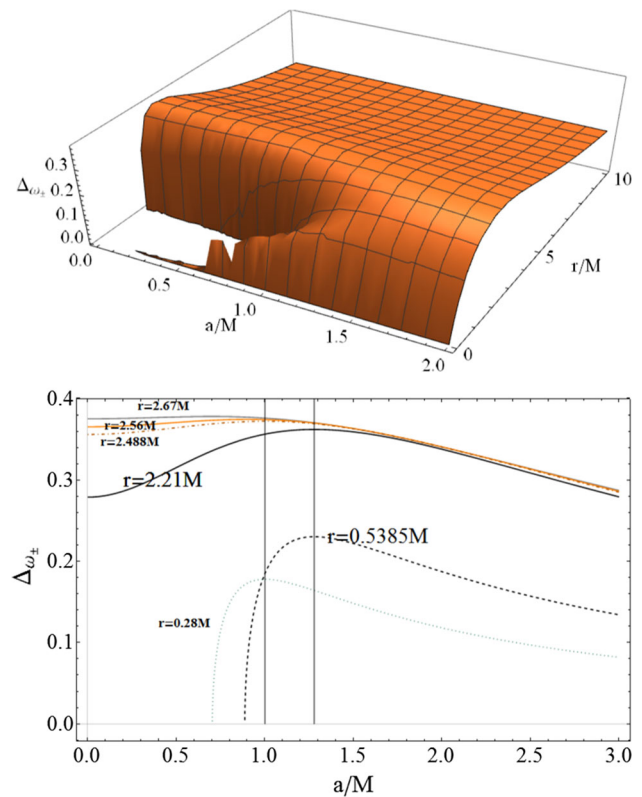

Fig. 7 Upper panel: plot of the frequency interval $\Delta\omega_\pm = \omega_+ - \omega_-$ as a function of the radius r/M and the **BH** and **NS** spin a/M. The extrema $r_\Delta^\pm$ and $r_\blacksquare^\pm$ are solutions of $\partial_r \Delta\omega_\pm = 0$ and $\partial_a \Delta\omega_\pm = 0$, respectively. Lower panel: the frequency interval $\Delta\omega_\pm = \omega_+ - \omega_-$ as a function of a/M for selected values of the orbit radius r/M; the maximum points are for the radii $r_\Delta^\pm$ or $r_\blacksquare^+$ – see Fig. 8

which is a function of the radial distance from the source and of the attractor spin. Figure 7 show the frequency interval $\Delta_{\omega_\pm}$ as a function of r/M and a/M.

An analysis of this quantity makes it possible to derive some key features about the eligible frequencies. For convenience, we present in Table 1 some special values of the spin-mass ratio, which we will consider in the following analysis. We summarize the obtained results in the following way:

Firstly, for any **NS** source with $a > a_\Delta \equiv 1.16905M$, the interval $\Delta_{\omega_\pm}$ increases as the observer (on the equatorial plane) moves inside the ergoregion Σ_ε^+ towards the static limit.

Secondly, in the case of **NS** geometries with $a \in]M, a_\Delta[$, i.e., belonging partially to the class of **NSI** spacetimes, the situation is very articulated. There is a region of maximum and a minimum frequencies, as the observer moves from the source towards the static limit. This phenomenon involves an orbital range partially located within the interval $]\hat{r}_-, \hat{r}_+[$, which is characterized by the presence of counterrotating circular orbits with negative orbital angular momentum $\mathscr{L} = -\mathscr{L}_-$ (cf. Fig. 8, where the radii $\hat{r}_\pm$ are plotted.).

For the maximum spin, $a = a_\Delta$, we obtain $\omega^+ = \omega^-$ on the radius $r \equiv r_\Delta^\pm(a_\Delta) = 0.811587M$ and, therefore, the range of possible frequencies for stationary observers vanishes. The points $r_\Delta^\pm(a)$ represent the extrema of the interval $\Delta_{\omega_\pm}$, i.e., the solutions of the equation $\partial_a \Delta_{\omega_\pm} = 0$ – Fig. 8. This property is present *only* in the case of **NS** geometries. In fact, there are the two critical orbits $r_\Delta^+ > r_\Delta^-$ and $r = r_\Delta^\pm(a_\Delta)$, which are the boundaries of a closed region, whose extension reaches a maximum in the case of the extreme Kerr geometry $a = M$, and is zero for $a = a_\Delta$. For $r \in]r_\Delta^-, r_\Delta^+[$, the separation parameter $\Delta_{\omega_\pm}$ decreases with the orbital distance, then on the inner radius r_Δ^- it reaches a maximum value, whereas on the outer radius r_Δ^+ it reaches a minimum. In the outer regions, at $r > r_\varepsilon^+$, the separation parameter increases with the distance from the source. This feature constitutes therefore a major difference in the the behavior of stationary observers within and outside the ergoregion of a naked singularity spacetime. However, a deeper analysis of the equatorial plane, outside the static limit, shows the existence of a second region for light surfaces in the **NS** case.

Table 1 Classes of **BH** and **NS** geometries according to their specific spins. The radii (r_γ^-, r_{mso}^-) corresponds to the photon circular orbit (or also last circular orbit) and the marginally stable circular orbit, respectively, for corrotating orbits in **BH** geometries. The **NS** case is char- acterized by the zero angular momentum radii $(\mathcal{L}(\hat{r}_\pm) = 0)$ and the radius of the marginally stable circular orbit $r_{mso}^{(NS)-} \in \Sigma_\varepsilon^+$. The explicit expressions for these radii can be found in [52–55,76]

Black hole classes: BHI : $[0, a_1[$,   **BHII** : $[a_1, a_2[$,   **BHIII** : $[a_2, M]$
$a_1/M \equiv 1/\sqrt{2} \approx 0.707107 : r_\gamma^-(a_1) = r_\varepsilon^+$, $a_2/M \equiv 2\sqrt{2}/3 \approx 0.942809 : r_{mso}^-(a_2) = r_\varepsilon^+$
Naked singularity classes: NSI : $]M, a_3]$,   **NSII** : $]a_3, a_4]$,   **NSIII** : $]a_4, +\infty]$
$a_3/M \equiv 3\sqrt{3}/4 \approx 1.29904 : \hat{r}_+(a_3) = \hat{r}_-(a_3)$, $a_4/M \equiv 2\sqrt{2} \approx 2.82843 : r_{mso}^{(NS)-}(a_4) = r_\varepsilon^+$

On the other hand, the angular velocity ω_- decreases with the orbit in the Kerr spacetime. The maximum frequency ω_+ also decreases in the **NS** spacetimes. In the **BH** cases, the angular velocity is always increasing for sources of the class **BHI**, while for the other sources there is a maximum for the velocity ω_+ at $r = r_\gamma^-$, which is the circular orbit of a photon or null-like particle corotating with the source. Such a kind of orbit, contained in Σ_ε^+, is a feature of the **BHII-III** spacetimes [2], this is also know as marginally or last circular orbit as no circular particle motion is possible in the region $r < r_\gamma^-$. We close this section with a brief discussion on the variation of the frequency interval $\Delta_{\omega_\pm}$, following a spin transition with $a > 0$. In the case of a singularity spin-transition, there are two extreme radii for the frequency interval

$$r_\blacksquare^+ \equiv \eta \cos\left[\frac{1}{3}\arccos\left(-\frac{8a^2}{\eta^3}\right)\right],$$

$$r_\blacksquare^- \equiv \eta \sin\left[\frac{1}{3}\arcsin\left(\frac{8a^2}{\eta^3}\right)\right],   \eta \equiv \frac{2\sqrt{8M^2 - a^2}}{\sqrt{3}},$$

$$\text{or alternatively}   a = \sqrt{-\frac{r(r^2 - 8M^2)}{r + 2M}}$$

$$\text{for}   r \in]0, 2\sqrt{2}M[, \tag{20}$$

where $r_\blacksquare^\pm : \partial_a \Delta_{\omega_\pm}|_{r_\blacksquare^\pm} = 0$ are maximum points – see Figs. 7 and 8.

3.2 Light surfaces

In this section, we briefly study the conditions for the existence of *light surfaces* and and their morphology. The condition (8), for the definition of a stationary observer, can be restated in terms of the solutions $r_s^\pm$, considering ω as a fixed parameter. Therefore, we now consider the solutions $r_s^\pm$ of the equation for the light surfaces defined in Eq. (9) in terms of the Killing null generator $\mathcal{L}_\pm$, as functions of the frequency ω. We obtain

$$\frac{r_s^-}{M} \equiv \frac{2\beta_1 \sin\left(\frac{1}{3}\arcsin\beta_0\right)}{\sqrt{3}},$$

$$\frac{r_s^+}{M} \equiv \frac{2\beta_1 \cos\left(\frac{1}{3}\arccos(-\beta_0)\right)}{\sqrt{3}}$$

where $\beta_1 \equiv \sqrt{\frac{1}{\omega^2} - \frac{1}{\omega_0^2}},   \beta_0 \equiv \frac{3\sqrt{3}\beta_1\omega^2}{\left(\frac{\omega}{\omega_0} + 1\right)^2}, \tag{21}$

where $\omega_0 \equiv M/a$ (cf. Eq. (10) and Fig. 2). For $\omega = 1/2$, in the limiting case of $a = M$, we have that $\omega_n = \bar{\omega}_n = \omega_h = 1/2$ and $r_s^\pm = M$ – see Figs. 2, 4 and 6.[10] Thus, there are solutions $r_s^+ = r_s^- = 0$ for $a \in]0, M[$ if $\omega \in (\omega_n, \bar{\omega}_n)$ where (for simplicity we use a dimensionless spin $a \to a/M$)

$$\bar{\omega}_n \equiv \frac{9 - a^2 + 6\sqrt{9 - 5a^2}\cos\left[\frac{1}{3}\arccos\alpha\right]}{a(a^2 + 27)} \tag{22}$$

$$\omega_n \equiv \frac{9 - a^2 - 6\sqrt{9 - 5a^2}\sin\left[\frac{1}{3}\arcsin\alpha\right]}{a(a^2 + 27)} \tag{23}$$

$$\alpha \equiv \frac{a^4 - 36a^2 + 27}{\left(9 - 5a^2\right)^{3/2}} \tag{24}$$

The situation is summarized in Table 2. We see that $\omega_n = \omega_+^\varepsilon$ for $a = a_1, \omega_n = \bar{\omega}_n = \omega_h = 1/2$ at[11] $a = M, \omega_+^\varepsilon = \omega_h$ at $a = a_s \equiv \sqrt{2\left(\sqrt{2} - 1\right)}M \approx 0.91017M$ and $a = 0$ (the static solution). Moreover, we have that $\omega_0 > \bar{\omega}_n > \omega_n > \omega_+^\varepsilon$ and $\omega_n > \omega_h$ for **BH**-sources, where $\omega_h > \omega_+^\varepsilon$ for $a \in]a_s, M]$. In the **NS** case, there are no crossing points for the radii $r_s^\pm$ and $\omega_0 > \omega_+^\varepsilon$ (see Fig. 4). The shrinking of the frequency interval $]\omega_-, \omega_+[$ is also shown in Figs. 6, 9 and 10, where the radii $r_s^\pm$ are also plotted as functions of the frequencies.

Figures 4, 5, and 6 contain all the information about the differences between black holes with $a < M$, and the case of naked singularities with $a > M$. We summarize the situation in the following statements:

---

[10] More precisely, it is $r_s^+ = r_s^- = 0$ for $a > 0$ and $\omega = \omega_0$. Also, $r_s^+ = r_s^- > r_+$ for $a = 0$ and $\omega = \pm\frac{1}{3\sqrt{3}}$. In the extreme Kerr spacetime geometry, we have that $r_s^+ = r_s^- > 0$ for $a = M$, $\omega = 1/2$ for $r = M$, and $\omega = -1/7$ for $r = 4M$. For a Kerr geometry, where $a/M \in]0, 1[$, it is $r_s^+ = r_s^- > r_+$ for $\omega = \omega_n$ or $\bar{\omega}_n$ (one positive and one negative value solution), while in the naked singularity case where $a > M$, the condition $r_s^+ = r_s^- > 0$ is valid only for one negative frequency – see Figs. 5 and 6.

[11] For a closer look at the role of this special frequency we note that $\bar{\omega}_n = \omega_n = \omega_h = 1/2$ at $a = M$ and, clearly, $\omega_0 = 1/2$ for $a = 2M$. We refer then to Figs. 3, 4, 5, 6, and 9.
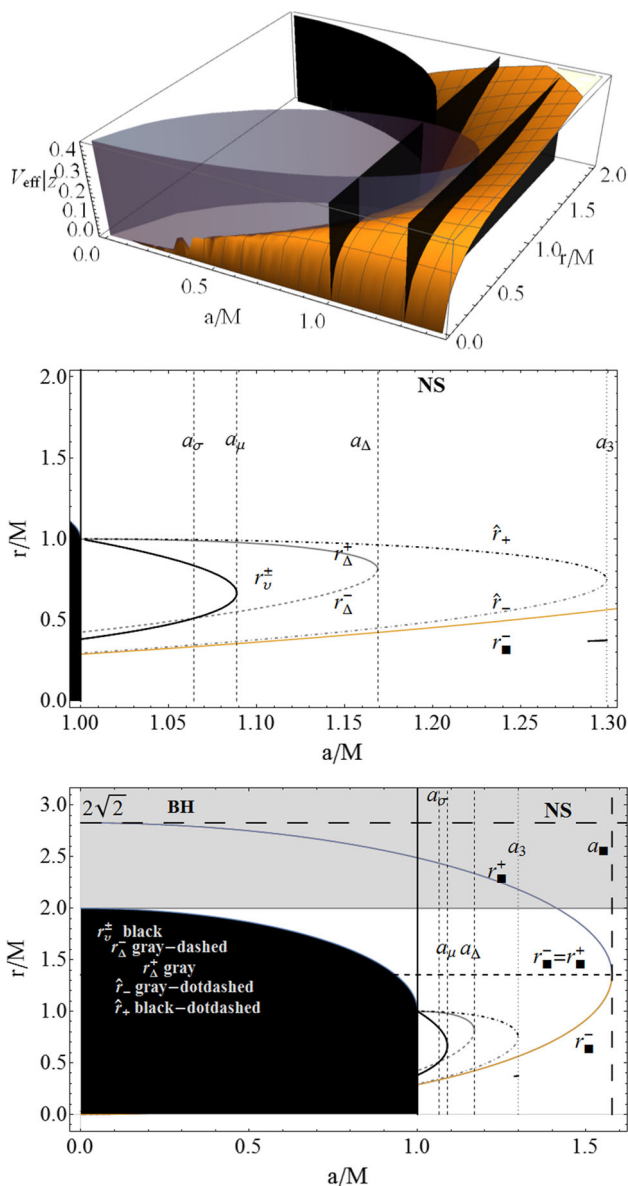
Fig. 8 Upper panel: the effective potential $V_{eff}|_Z$ for the ZAMOS $\mathscr{L} = 0$, for **BH** and **NS** sources as a function of the source spin a/M and the radius r/M. The effective potential function is the value of $\mathscr{E}/\mu$ at which the (radial) kinetic energy of the particle vanishes. Black planes represent the spin values $a = M$, extreme Kerr **BH**, and $a_3 \equiv 3\sqrt{3}/4M$, a **NS** geometry, where $\hat{r}_- = \hat{r}_+$. The orbits $\hat{r}_- \leq \hat{r}_+$, gray surfaces, are for $a < M$ (**BH**-case) inside the horizon ($r < r_+$). The inner black surface is the horizon r_+. Central panel: the radius $r(a)$, solution of $\partial_r \Delta_{\omega_\pm} = 0$, i.e., it represents the critical points of the separation parameter $\Delta_{\omega_\pm} \equiv (\omega_+ - \omega_-)|_{\pi/2}$ on the equatorial plane $\theta = \pi/2$. The radius $r_v^\pm$, where the orbital energy $\mathscr{E} = 0$, and the orbits $\hat{r}_\pm$, for which $\mathscr{L} = 0$, are also plotted. Dashed lines represent the spins $a_\sigma = 1.064306M$, $a_\mu = 4\sqrt{2/3}/3M \approx 1.08866M$, $a_\Delta = 1.16905M$ and $a_3 = 3\sqrt{3}/4M$. The black region corresponds to $r < r_+$. Bottom panel: the radii $r_\blacksquare^\pm : \partial_a \Delta_{\omega_\pm} = 0$ are plotted as functions of a/M – see also Fig. 7

Naked singularities spacetimes: For $a > M$, the solutions for the equation of the light surfaces in the limiting case $\omega = 0$ (static observer) are located at $r = r_\varepsilon^+$. While

for any frequency within the range $\omega \in]0, \omega_+^\varepsilon[$ there is one solution r_s^-, for larger frequencies in the range $\omega \in [\omega_+^\varepsilon, \omega_0[$ there are two solutions $r_s^\pm$. In the ergoregion Σ_ε^+ of a naked singularity, there exists a limit $\omega_0 \equiv M/a$ for the angular frequency.

Extreme black hole spacetime: For $a = M$, we obtain the following set of solutions $(\omega = 0, r = r_\varepsilon^+)$, $(\omega \in]0, 1/3[, r = r_s^-)$, and $(\omega \in [1/3, 1/2[, r = r_s^\pm)$.

Black hole spacetimes: We consider first the class **BHI** with $a \in]0, a_1[$. In the limit $\omega = 0$, there exists a solution for the light surface with $r = r_\varepsilon^+$. More generally, the solutions are constrained by the following set of conditions:

$$\mathfrak{C}_1 : \quad \omega \in]0, \omega_+^\varepsilon] \cup \omega \neq \omega_h \quad \text{with solution } r = r_s^-.$$
(25)

$$\mathfrak{C}_2 : \quad \omega \in [\omega_+^\varepsilon, \omega_n[\quad \text{with solution} \quad r = r_s^\pm, \quad (26)$$
$$\omega = \omega_n, \quad \text{with solution} \quad r = r_s^-. \quad (27)$$

Then, we consider **BH** spacetimes with spin $a \in]a_1, a_s[$, where $a_s \equiv \sqrt{2(\sqrt{2}-1)}M < a_2$. These spacetimes include a part of **BHII**-sources and the condition $\mathfrak{C}_1$ applies.

For spacetimes with rotation $a = a_s$, the conditions $\mathfrak{C}_1$ and $\mathfrak{C}_2$ apply. Then, in the special case $\omega_+^\varepsilon = \omega_h$ or $\omega = \omega_+^\varepsilon$, there is a solution with $r = r_s^+$.

Finally, for spacetimes with $a \in]a_s, M[$, which belong to the class of **BHII** and **BHIII** sources, the condition $\mathfrak{C}_1$ holds, whereas the condition $\mathfrak{C}_2$ applies for frequencies within the interval $\omega_h < \omega_n$. Finally, in the special case $\omega = \omega_h$, there is one solution at $r = r_s^+$, and for $\omega = \omega_n$ we have the solution $r = r_s^-$.

A summary and comparison of these two cases is proposed also in Figs. 5 and 6, where the surfaces $r_s^\pm$ are studied as functions of a/M and ω. It is evident that the extreme solution $a/M = 1$ is a limiting case of both surfaces $r_s^\pm$, varying both in terms of the spin and the angular velocity ω. Thus, the difference between the regions where stationary observers can exist in the **BH** case (gray regions in Fig. 6) and in the **NS** case are clearly delineated. In **BH** spacetimes, the surfaces $r_s^\pm$ are confined within a restricted radial and frequency range. On the other hand, in the naked singularity case, the orbits and the frequency range is larger than in the black hole case. Moreover, the surfaces $r_s^\pm$ can be closed in the case of **NS** spacetimes, inside the ergoregion, for sufficiently low values of the spin parameter, namely $a \in]M, a_4[$. Furthermore, in any Kerr spacetime, there is a light surface at $r_s^\pm = r_\varepsilon^+$ with $\omega = M/a_4$. In Sect. 4, we complete this analysis by investigating the special case of zero angular momentum observers,

Table 2 Existence of stationary observers in **BH** and **NS** spacetimes, respectively. The spin/mass ratio a/M, angular frequencies ω and orbital ranges r are listed. See also Fig. 4

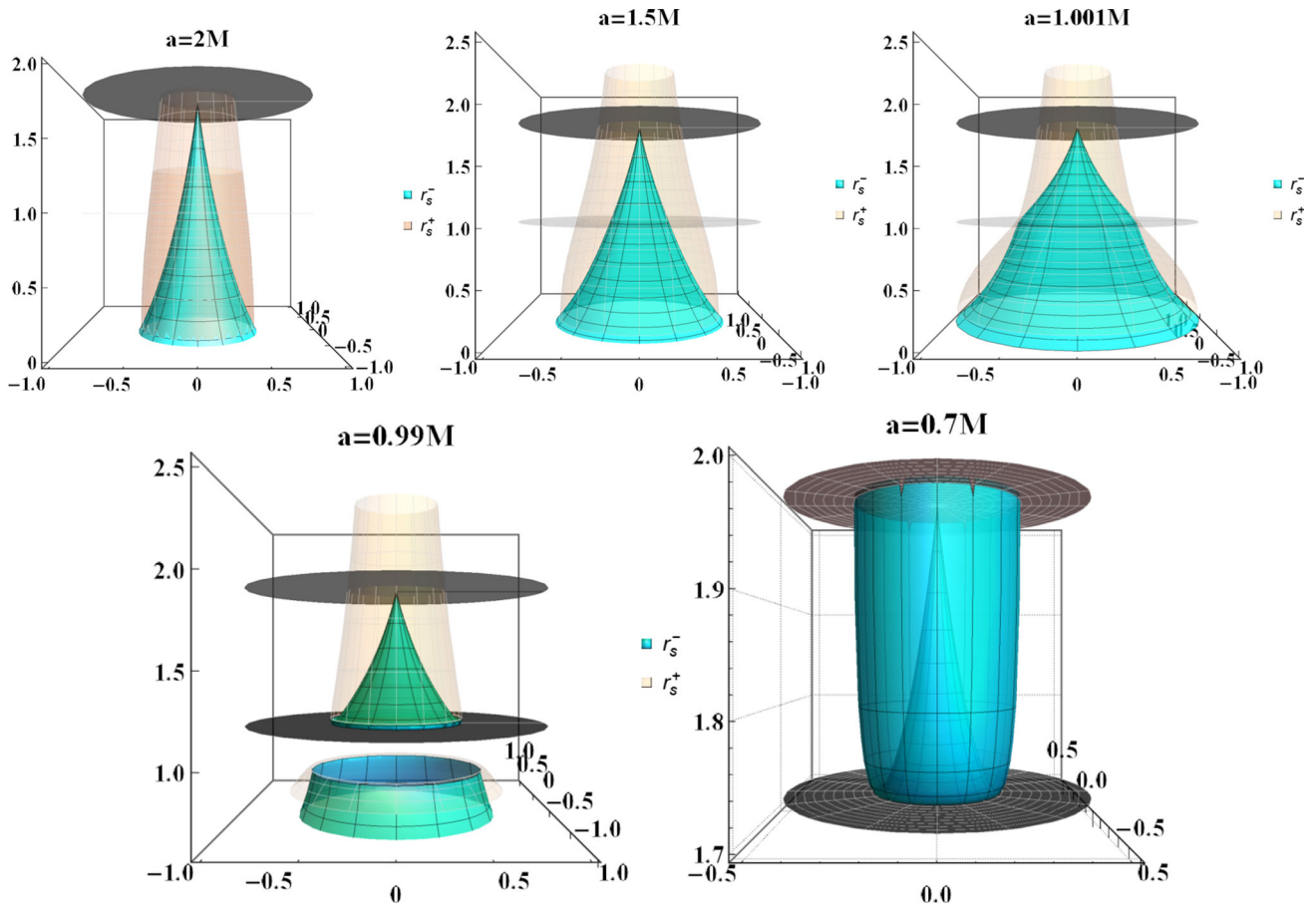| Black holes			Naked singularities		
$a \in]0, a_1]$	$\omega \in]0, \omega_+^\varepsilon[$	$r \in]r_s^-, r_\varepsilon^+]$	$a > M$	$\omega \in]0, \omega_+^\varepsilon[$	$r \in]r_s^-, r_\varepsilon^+]$
$a \in]a_1, M]$	$\omega \in]0, \omega_+^\varepsilon[$	$r \in]r_s^-, r_\varepsilon^+]$		$\omega = \omega_+^\varepsilon$	$r \in]r_s^-, r_\varepsilon^+[$
	$\omega = \omega_+^\varepsilon$	$r \in]r_s^-, r_\varepsilon^+[$		$]\omega_+^\varepsilon, \omega_0[$	$r \in]r_s^-, r_s^+[$
	$\omega \in]\omega_+^\varepsilon, \omega_n[$	$r \in]r_s^-, r_s^+[$			

Fig. 9 Plots of the surfaces $r_s^\pm$ (in units of mass) versus the frequency ω for different spin values a/M, including **BH** and **NS** geometries – see also Fig. 6. The surfaces $r_s^\pm$ are represented as revolution surfaces with height $r_s^\pm$ (vertical axes) and radius ω (horizontal plane). Surfaces are generated by rotating the two-dimensional curves $r_s^\pm$ around an axis (revolution of the function curves $r_s^\pm$ around the "z" axis). Thus,

$r =$ constant with respect to the frequency ω is represented by a circle under this transformation. The disks in the plots are either $r = M$, $r = r_+$ or $r = r_\varepsilon^\pm = 2M$. The surfaces $r_s^\pm$ are green and pink colored, respectively (as mentioned in the legend). In the last panel ($a = 0.7M$), both radii $r_s^\pm$ are green colored

and we find all the spacetime configurations in which they can exist.

4 Zero angular momentum observers

This section is dedicated to the study of zero angular momentum observers (ZAMOs) which are defined by the condition

$$\mathscr{L} \equiv u_\alpha \xi_{(\phi)}^\alpha = g_{\alpha\beta} \xi_\phi^\alpha p^\beta = g_{t\phi} \dot{t} + g_{\phi\phi} \dot{\phi} = 0. \tag{28}$$

In terms of the particle's four-velocity, the condition $\mathscr{L} = 0$ is equivalent to $d\phi/dt = -g_{\phi t}/g_{\phi\phi} \equiv \omega_Z = (\omega_+ + \omega_-)/2$, where the quantity ω_Z is the ZAMOs angular velocity introduced in Eq. (8), and the frequency of arbitrary stationary observers is written in terms of ω_Z [2]. The sign of ω_Z is in concordance with the source rotation. The ZAMOs angular velocity is a function of the spacetime spin (see Figs. 11 and 12, where constant ZAMOs frequency profiles are shown). In the plane $\theta = \pi/2$, we find explicitly
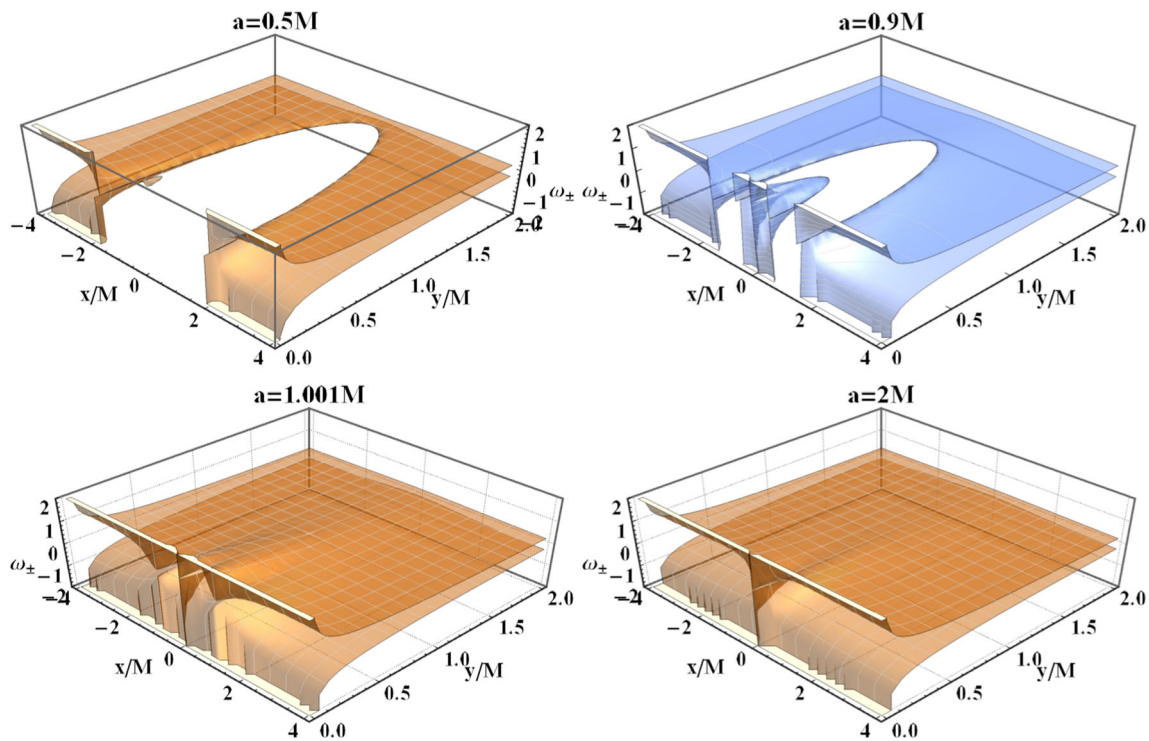
Fig. 10 Plots of frequency surfaces $\omega_\pm(r,\theta)$ as functions of the radial distance r in Cartesian coordinates (x,y) for different spin values a, including **BH**s and **NS**s – see also Fig. 6
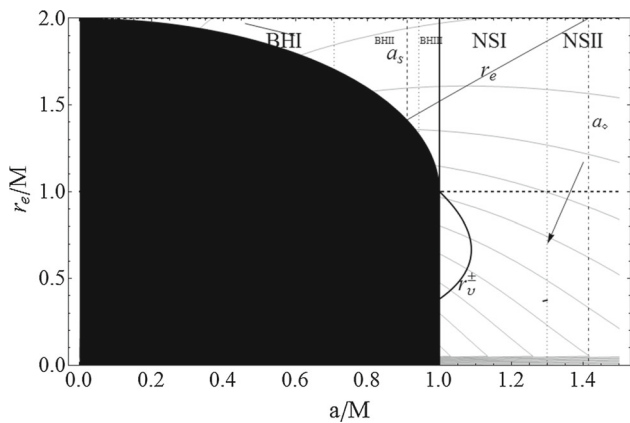

Fig. 11 The plot shows the orbits (gray curves) of constant ZAMOs velocity ω_Z =constant in the **BH** and **NS** regions. The radius r_e and the spin a_s : $r_e = r_+$ are marked by dashed lines. The arrows show the increasing of the angular velocity

$$\omega_Z|_{(\theta=\pi/2)} = \frac{2aM^2}{r^3 + a^2(r + 2M)}. \tag{29}$$

As discussed in [2,54,55], ZAMOs along circular orbits with radii $\hat{r}_\pm$ are possible only in the case of "slowly rotating" naked singularity spacetimes of class **NSI**. This is a characteristic of naked singularities which is interpreted generically as a repulsive effect exerted by the singularity [52–55,76]. On the other hand, $\omega_Z^2 = \omega_*^2$ for $r = r_\pm$, while $\omega_Z^2 > \omega_*^2$

in the region $r > r_+$ for **BH** spacetimes, and in the region $r > 0$ for **NS** spacetimes (see also Fig. 12).

ZAMOs angular velocity and orbital regions

The ZAMOs angular velocity ω_Z is always positive for $a > 0$, and vanishes only in the limiting case $a = 0$. This means that the ZAMOs rotate in the same direction as the source (dragging of inertial frames).

As can be seen from Eq. (29), the frequency ω_Z for a fixed mass and $a \neq 0$ is strictly decreasing as the radius r/M increases.

For the **NS** regime it is interesting to investigate the variation of **ZAMO** frequency ω_Z on the orbits $\hat{r}^\pm$. These special radii of the **NS** geometries do not remain constant under a spin-transition of the central singularity. We shall consider this aspect focusing on the curves $\hat{r}^\pm(a)$ of the plane $r - a$ as illustrated in Fig. 8. This will enable us to evaluate simultaneously the frequency variation on these special orbits, following a spin variation of the naked singularity in the rage of definition of $\hat{r}^\pm$, and to evaluate the combined effects of a variation in the orbital distance from the singularity and a change of spin. A similar analysis will be done, from a different point of view, also for stationary observers.

In $\Sigma_\varepsilon^\pm$, the velocity $\omega_Z = \hat{\omega}^-$ (in NSs) always *decreases* with the orbital radii $\hat{r}^-$, i.e. $\partial_{\hat{r}}\hat{\omega}^- < 0$, when the spin increases, i.e. $\partial_a\hat{r}^- > 0$ (see Figs. 8 and 12). As $\hat{r}^+$ mono-
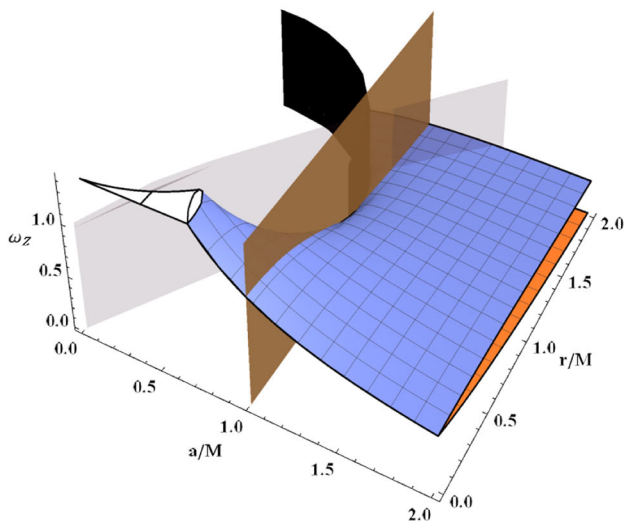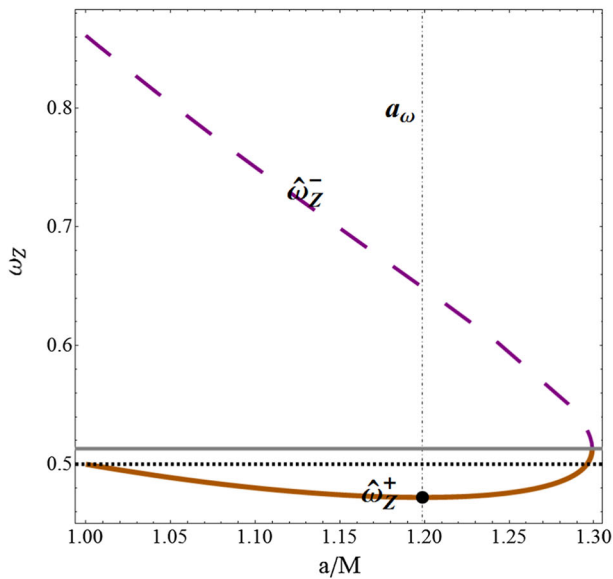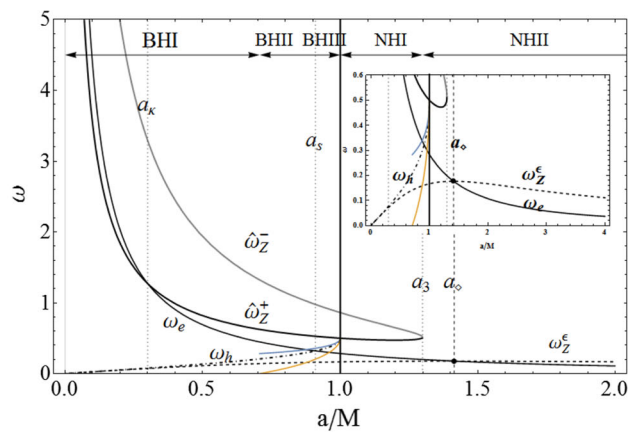
◀ **Fig. 12** Upper panel: the angular velocity $\omega_e \equiv \omega_Z(r_e)$ as a function of a/M. The angular velocities $\omega_Z^\varepsilon \equiv \omega_Z(r_\varepsilon^+)$ (dashed curve), $\omega_h \equiv \omega_\pm(r_+) = \omega_Z(r_+)$ (dot-dashed curve), $\hat\omega_Z^\pm \equiv \omega_Z(\hat{r}_\pm)$ as functions of the spacetime rotation a/M for different **BH** and **NS** classes. Dotted lines are $a_\kappa \approx 0.3002831060M : \omega_e = \hat\omega_Z^+$, $a_s \approx 0.91017M : \omega_e = \omega_h$, $a_3 : \hat\omega_Z^+ = \hat\omega_Z^- = 8/9\sqrt{3}$, and finally the spin $a_\diamond : \sqrt{2}M : \omega_Z^\varepsilon = \omega_2$ (dashed line) which is a maximum for ω_Z^ε (the maximum point is marked with a point). The inset plot is a zoom. The radius r_e/M is a maximum for ω_e. The angular velocities $\omega_\pm$ on the **BH** photon orbit $r_\gamma \in \Sigma_\varepsilon^+$ are also plotted (colored lines). Center panel: $\hat\omega_Z^\pm \equiv \omega_Z(\hat{r}_\pm)$ as functions of a/M for different **NS** classes. The minimum point of the ZAMOs frequency $\hat\omega_Z^+$ is marked with a point at spin $a_\omega = 1.19866M$. Bottom panel: the ZAMOs angular velocity ω_Z is plotted as a function of the spin a/M and the radius r/M. The plane $a = M$ and the horizon surface $r = r_+$ are black surfaces. The gray surface denotes the orbit r_e. For both **NS** and **BH** spacetimes, the ZAMOs have a maximum frequency which is a function of a/M. The black thick curve corresponds to $\mathscr{E} = 0$. The black region denotes the region inside the outer horizon $r < r_+$

therefore, the special value $a_\omega = 1.1987M$ is a minimum point of the ZAMOs frequency $\hat\omega_Z^+$ – see Fig. 12. *Viceversa*, as $\hat{r}^-$ increases after a **NS** spin-up, the corresponding ZAMOs frequency $\hat\omega^- = \omega_Z(\hat{r}^-)$ decreases as the observer moves along the curve $\hat{r}^-(a)$. Thus, we can say that, if the **NS** spin increases, the frequency $\hat\omega^+$ decreases, approaching, but never reaching, the singularity, i. e., $\partial_a \hat{r}^+ < 0$ for $a \in [M, a_\omega[$. *Viceversa*, increasing the **NSs** spin in spacetimes with $a \in]a_\omega, a_3[$, the frequency $\hat\omega^+$ increases again and the orbit $\hat{r}^+$ moves towards the central singularity. On the other hand, the frequency $\hat\omega^-$ monotonically decreases with the naked singularity spin, i.e. $\partial_a \hat{r}^- > 0$; therefore, for a fixed **NS** spin, the frequency interval decreases, i.e. $\hat\omega^- > \hat\omega^+$. In fact, the velocity ω_Z is strictly *decreasing* with the radius r in the **BH** and **NS** regimes with $a \neq 0$ (i.e. $\partial_r \omega_Z < 0$). Moreover, in general ω_Z increases as the observer approaches the black hole at fixed spin, and it decreases as the observer moves far away from the center of rotation.

In the static limit, we have that $\omega_Z(r_\varepsilon^+) = \omega_+^\varepsilon/2$. In fact, the asymptotic behavior of the frequency is determined by the relations

$$\lim_{r \to r_+} \omega_Z = \lim_{r \to r_+} \omega_\pm = \omega_h,$$
$$\lim_{r \to +\infty} \omega_Z = 0, \quad \lim_{r \to 0} \omega_Z = \omega_0. \qquad (30)$$

Change in the intrinsic spin

The angular velocity of the ZAMOs inside Σ_ε^+ varies according to the source spin. This might be especially important in a possible process of spin-up or spin-down as a result of the interaction, for example, with the surrounding matter. In [2], this phenomenon and its implications were investigated, considering different regions close to the singularity. For a fixed orbital radius r, the ZAMOs angular velocity strongly depends on the value of the spacetime spin-mass ratio. In

tonically decreases with the spin during a **NS** spin-up process (see Fig. 8), the frequency $\hat\omega^+ = \omega_Z(\hat{r}^+)$ decreases in the spin-range $a \in [M, a_\omega[$, and increases in the range $]a_\omega, a_3]$;

particular, depending on the value of the ratio a/M, there can exist a radius of maximum frequency r_e given by

$$r_e \equiv \frac{\sqrt[3]{3}a^2 + \Upsilon^2}{3^{2/3}\Upsilon},$$

$$\Upsilon \equiv \sqrt[3]{9Ma^2 + \sqrt{3}\sqrt{a^4\left(27M^2 - a^2\right)}} \qquad (31)$$

that are solutions of the equation $\partial_a \omega_Z|_{\pi/2} = 0$ at which the frequency is denoted by $\omega_e \equiv \omega_Z(r_e)$ (see Figs. 11, 12). A detailed analysis of the expression for the radius r_e shows that in can exist in spacetimes that belong to the class **BHII** with spin $a = a_s$, where $r_e(a_s) = r_+(a_s)$, and to the classes **BHIII**, **NSI**, and **NSII** with the limiting value $a = a_\diamond = \sqrt{2}M$, where $a_\diamond : r_e = r_\varepsilon^+$ (see Figs. 2, 11). Spacetimes with spin a_s belong to the class **BHII**, as defined in Table 2, and have been analyzed in the context of stationary observers in Sects. 3.1 and 3.2 (Figs. 4, 11, 12 and 13 show the behavior of several quantities related to ZAMOs in relation to other frequencies.). In this particular case, we have that

$$\omega_+^\varepsilon = \omega_h = 0.321797 \quad \text{and} \quad r_e(a_s) = r_+(a_s). \qquad (32)$$

We focus our attention on ergoregion Σ_ε^+, bounded from above by the radius r_ε^+ and from below by $r = 0$ and $r = r_+$ for **NSs** and **BHs**, respectively. We consider the role of the radius r_e, as the maximum point of the ZAMO frequency, as a function of the source spin-mass ratio. Thus, for black holes with $a \in [0, a_s]$, the frequency ω_Z increases with a/M always inside the ergoregion; this holds for any orbit inside Σ_ε^+ (i.e. for a fixed value $\bar{r} \in \Sigma_\varepsilon^+$, if a **BH** spin-up shift occurs in the range $[0, a_s]$, the function $\omega_Z(\bar{r}, a)$ increases with $\bar{r}$). For spins $a \in]a_s, M]$, instead, the frequency ω_Z grows with the spin only for $\bar{r} \in]r_e, r_\varepsilon^+[$; on the contrary, for radii located close to the horizon, $\bar{r} \in]r_+, r_e]$, $\omega_Z(\bar{r}, a)$ *decreases* following a spin up in the range $\in]a_s, M]$ (i.e, $\partial_a r_+ < 0$ and $\partial_a r_e > 0$). In the case of **NS**-spacetimes, the frequency $\omega_Z(\bar{r}, a)$ is an increasing function of the dimensionless spin in the **NS** spin range $]M, a_\diamond[$ and on the orbit $\bar{r} \in]r_e, r_\varepsilon^+]$. Moreover, the frequency $\omega_Z(\bar{r}, a)$ decreases with the spin in the range of values $a \in]M, a_\diamond[$ and on $\bar{r} \in]0, r_e]$. This situation is distinctly different for **NS** with $a > a_\diamond$, for which in the ergoregion an increase of the spin corresponds to a decrease of ω_Z. This is an important distinction between different **NS** regimes.

We note that $r_e(a_s) = r_+(a_s)$ for the spin $a_s = \sqrt{2\left(\sqrt{2} - 1\right)}M$ (see Fig. 11). Moreover, in **NSII** naked singularity spacetimes with spin $a_\diamond = \sqrt{2}M : r_e = r_\varepsilon^+$, we obtain that $\omega_Z^\varepsilon = \omega_e$ – Fig. 12. Remarkably, the spin $a_\diamond$ is the maximum point of the frequency $\omega_Z^\varepsilon(a_\diamond) = \omega_e(a_\diamond) \equiv \omega_Z^{\varepsilon-Max} = 0.176777$ and also the maximum point of the frequency ω_+^ε (see Fig. 2). In other words, in naked singularity spacetimes with $a = a_\diamond$, where $r_e = r_\varepsilon^+$, the ZAMOs

frequency at the ergosurface ω_Z^ε reaches a maximum value which is equal to ω_e, defined through the radius in Eq. (31); moreover, the frequency ω_+^ε reaches its maximum value at the ergosurface.

ZAMOs energy

The circular motion of test particles can be described easily by using the effective potential approach [116]. The exact form of such an effective potential in the Kerr spacetime is well known in the literature (see, for example, [54,55]). The effective potential function $\mathcal{V}_{eff}^+$ represents the value of $\mathcal{E}/\mu$ that makes r into a turning point ($\mathcal{V}_{eff} = \mathcal{E}/\mu$), μ being the particle mass; in other words, it is the value of $\mathcal{E}/\mu$ (in the case of photons, μ shall depend on an affine parameter and the impact parameter $\ell \equiv \mathcal{L}/\mathcal{E}$ is relevant for the analysis of trajectories) at which the (radial) kinetic energy of the particle vanishes. This can easily be obtained from the geodesic equations with the appropriate constraints or through the normalization conditions of the four-velocities, taking into account the constraints and the constants of motion [116]. Here we consider specifically an effective potential associated to the ZAMOs.

The orbits $\hat{r}_\pm$ are critical points of the effective potential, i. e., $\hat{r}_\pm : \partial_r V_{eff}|_Z^2 = 0$. Here we consider for the ZAMO $V_{eff}|_Z^2 = \tilde{\kappa} g_{\phi\phi}[\omega_*^2 - \omega_Z^2]$ where $\tilde{\kappa}$ is a factor related to the normalization condition of the ZAMO four-velocity ($\tilde{\kappa} = -1$ for timelike ZAMOs, where $u^\phi = -\omega_Z u^t$ and $u^t = -\varepsilon \mathcal{E}/g_{\phi\phi}[\omega_*^2 - \omega_Z^2]$, $\varepsilon = 1$ according to Eq. (3); in the ergoregion $V_{eff}|_Z^2 > 0$, but $V_{eff}|_Z^2 = 0$ for $r = 0$ and $r = r_+$). The energy E of the ZAMOs is always positive for both **BH** and **NS** spacetimes, and it grows with the source spin; in fact, solutions for $V_{eff}|_Z = 0$ are not possible because this would correspond to the case of a null angular momentum with null energy. The energy on the orbits $\hat{r}_\pm$ where $\mathcal{L} = 0$ is always positive. In **BH** geometries, the potential $\mathcal{V}_{eff}$, at $\mathcal{L} = 0$, increases with the distance from the source and has no critical points as a function of r/M. The most interesting case is then for the slow naked singularity spacetimes of the first class, **NSI** with $a \in]M, a_1]$, where there is a closed and connected orbital region of circular orbits with $r \in]\hat{r}_-, \hat{r}_+[$. The radii $\hat{r}_\pm$ are ZAMOs orbits, and in this region the potential decreases with the orbital radius. However, in the outer region $r \in]r_+, \hat{r}_-[\cup]\hat{r}_+, 2M[$, the potential increases with the radius. This implies that the radii $\hat{r}_\pm$ are possible circular ZAMOs orbits. In fact, $\hat{r}_-$ is an *unstable* orbit and $\hat{r}_+$ is a *stable* orbit. Thus, in any geometry of this set, there is a stable orbit for the ZAMOs with angular velocity $\hat{\omega}_Z^\pm \equiv \omega_Z(\hat{r}_\pm)$ different from zero, where $\hat{\omega}_Z^- < \hat{\omega}_Z^+$ (see Fig. 12).

In [2], we investigated the orbital nature of the static limit. Here, in Fig. 13, the velocity ω_Z and the ratio $\mathcal{R}^\varepsilon \equiv \mathcal{E}_-^\varepsilon/\mathcal{L}_-^\varepsilon$
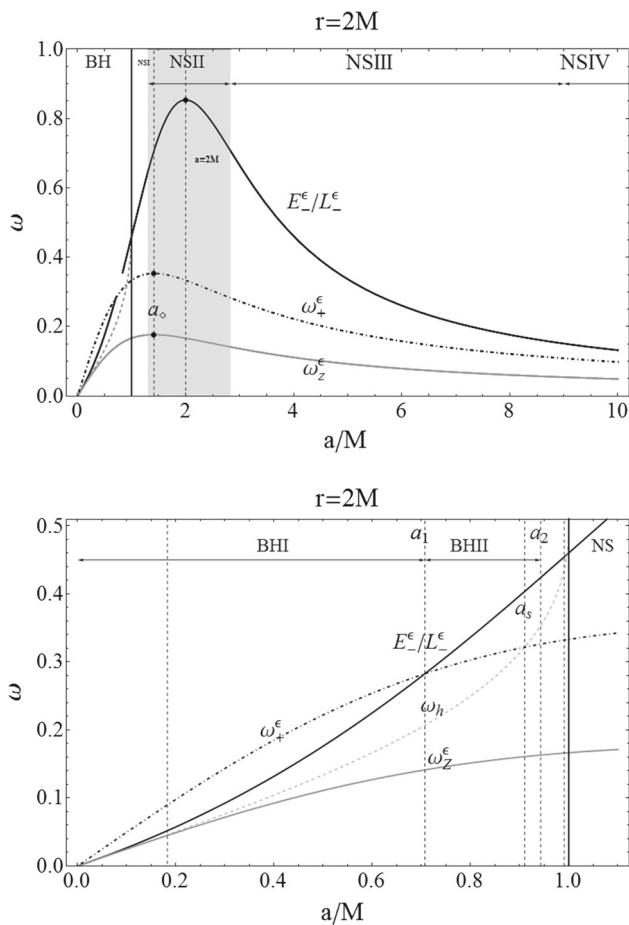
Fig. 13 Upper panel: the ratio $\mathscr{E}_-^\varepsilon/\mathscr{L}_-^\varepsilon$ and the angular momentum of the ZAMOs ω_Z^ε as a function of a/M in the static limit $r = r_\varepsilon^+$. The angular momentum $\omega_+^\varepsilon \equiv \omega_+(r_\varepsilon^+)$ which is a boundary frequency for the stationary observer (outer light surface) is plotted (gray curve). The radius r_ε^+ is defined by the condition $\omega_-(r_\varepsilon^+) = 0$, ω_h is the ZAMOs angular velocity on $r = r_+$, i.e. $\omega_\pm(r_\pm) = \omega_h$. The maxima are denoted by points. The **NSII** region is in light-gray. A zoom of this plot in the **BH** region is in the bottom panel

(that is, the inverse of the specific angular momentum defined as u_ϕ/u_t) are considered as functions of the source spin at the static limit. We explore the relation between the ZAMOs and the stationary observes, where $\omega_Z = (\omega_+ + \omega_-)/2$, for **NSI** sources at the static limit. A maximum value, $\mathscr{R}^\varepsilon = 0.853553M$, is reached at $a = 2M \in$ **NSII**. Also, a maximum value $\omega_Z^{\varepsilon-Max} = 0.176777$ exists for the ZAMOs angular velocity at $a = a_\diamond \in$ **NSII**. This ratio is always greater than the angular momentum of the ZAMOs at the static limit.

In **BH** spacetimes, the angular velocity for stationary observers is limited by the value ω_h which occurs for the radius r_+. We can evaluate the deviation of this velocity in a neighborhood of the radius r_+, since the four-velocity of the observers rotating with ω (where $u^a \equiv \xi_t + \omega\xi_\phi$) must be timelike outside the horizon and therefore it has to be

$\mathscr{R} = \mathscr{E}/\mathscr{L} > \omega_h$ in that range (the event horizon of a Kerr black hole rotates with angular velocity ω_h [1]). This limit cannot be extended to the case of naked singularities. However, one can set similarly the threshold $\mathscr{E} > \omega_a\mathscr{L}$ in the case of circular orbits, where the frequency limit is restricted to the values $\omega_a \in [1, a_\mu^{-1}M[$ as $\omega_a \in [\omega_0(a = M), \omega_0(a_\mu)[$.

5 Summary and conclusions

In this work, we carried out a detailed analysis of the physical properties of stationary observers moving in the ergoregion along equatorial circular orbits in the gravitational field of a spinning source, described by the stationary and axisymmetric Kerr metric. We derived the explicit value of the angular velocity of stationary observers and analyzed all possible regions where circular motion is allowed, depending on the radius and the rotational Kerr parameter. We found that in general the region of allowed values for the frequencies is larger for naked singularities than for black holes. In fact, for certain values of the radius r, stationary observers can exist only in the field of naked singularities. We interpret this result as a clear indication of the observational differences between black holes and naked singularities. Given the frequency and the orbit radius of a stationary observer, it is always possible to determine the value of the rotational parameter of the gravitational source. Our results show that in fact the probability of existence of a stationary observer is greater in the case of naked singularities that in the case of black holes. Moreover, it is possible to introduce a classification of rotating sources by using their rotational parameter which, in turn, determines the properties of stationary observers. Black holes and naked singularities turn out to be split each into three different classes in which stationary observers with different properties can exist. In particular, we point out the existence of weak (**NSI**) and strong (**NSIII**) naked singularities, corresponding to spin values close to or distant from the limiting case of an extreme black hole, respectively.

Light surfaces are also a common feature of rotating gravitational configurations. We derived the explicit value of the radius for light surfaces on the equatorial plane of the Kerr spacetime. In the case of black holes, light surfaces are confined within a restricted radial and frequency range. On the contrary, in the naked singularity case, the orbits and the frequency ranges are larger than for black holes. Again, we conclude that light surfaces can be found more often in naked singularities. The observation and measurement of the physical parameters of a particular light surface is sufficient to determine the main rotational properties of the spinning gravitational source. We believe that the study of light surfaces (defining the "throat" discussed in Sect. 3) has important applications regarding the possibility of directly observing a black hole in the immediate vicinity of an event horizon

(within the region defined by the static limit), as this seems to be possible in the immediate future through, for example, the already active Event Horizon Telescope (**EHT**) projects.[12]

We also analyzed the conditions under which a ZAMO can exist in a Kerr spacetime. In particular, we computed the orbital regions and the energy of ZAMOs. The frequency of the ZAMOs is always positive, i.e., they rotate in the same direction of the spinning source as a consequence of the dragging of inertial frames. The energy is also always positive. The most interesting case is that of slowly rotating naked singularities (**NSI**) where there exists a closed and disconnected orbital region. This particular property could, in principle, be used to detect naked singularities of this class. We derived the particular radius at which the frequency of the ZAMOs is maximal, showing that the measurement of this radius could be used to determine whether the spinning source is a black hole or a naked singularity and its class, according to the classification scheme formulated here. To be more specific, from Table 2 we infer that the existence of stationary observers in black hole spacetimes is limited from above by the frequency $\omega_+^{\mathscr{E}}$, which is the highest frequency on the static limit, implying the frequency lower bound $\omega = 0$ – see also Fig. 4. In this figure, we also show the maximum frequency, $\omega_{\mathscr{E}}^+$, at the static limit for a naked singularity with $a = a_\diamond = \sqrt{2}M \in$ **NSII**. This spin plays an important role for the variation of the ZAMOs frequency in **NSs** in terms of the singularity dimensionless spin – see Figs. 12 and 13. On the other hand, for strong **BHs**, with $a > a_1$, the frequency is bounded from below by $\omega = \omega_{\mathscr{E}}^+$ and from above by ω_n, as the radial upper bound is r_s^+. A similar situation occurs for **NSs**, provided that ω_n is replaced with the limiting frequency ω_0. The special role of the **BH** spin a_1 is related to the presence of the photon circular orbit in the **BH** ergoregion, which is absent in **NS** geometries; consequently, as seen in Table 2, there is no distinction between the naked singularities classes. However, the analysis of the frequencies in Fig. 4 shows differently that there are indeed distinguishing features in the corresponding ergoregions. In the case of naked singularities, the frequency range of stationary observers has as a boundary the outer light-surface, $r = r_s^+$, then it narrows as the spin increases, and finally vanishes near the static limit.

The frequency of the orbits on the static limit, in fact, converges to the limit $\omega_0 = M/a$, which is an important frequency threshold for the **NS** regime. The presence of a maximum for the special **NS** geometry with $a = a_\diamond$ on the static limit is symptomatic for the nature of this source – see Figs. 4, 6 and 13. The study of the surfaces $r_s^\pm$ on the plane (r, ω), for different values of the spin-mass ratio, shows a clear difference between the allowed regions in naked singularities and black holes (gray region in Fig. 6). There is an open "throat" between the spin values $a \lesssim M$ (strong

BHs) and $a \gtrsim M$ (very weak **NSs**), with an opening of the cusp (at $r = 0$ in these special coordinates) for the frequency $\omega = 0.5$. We note a change in the situation for spins in $a/M \in]1, 1.0001]$; this region is in fact extremely sensitive to a change of the source spin; the throat of $r_s^\pm$ has, in this special spin range, a saddle point around $(r = M, \omega = 1/2)$ between $[a_\mu, a_3]$, which is not present in stronger singularities. The spins in this range are related to the negative state energy and the radii $r_\upsilon^\pm$, where the orbital energy is $\mathscr{E} = 0$ – Fig. 8. Particularly, we point out the spin $a = a_\sigma = 1.064306M$, where $r_\upsilon^- = r_\Delta^- = 0.5107M$, for which at $r_\Delta^\pm$ there is a critical point of the frequency amplitude $\Delta\omega^\pm$. In **BH** geometries, the frequencies increase with the spin and with the decrease of the radius towards the horizon. The curves $r_s^\pm$ continue to increase with the presence of a transition throat at $r = M$ that increases, stretching and widening. This throat represents a "transition region" between **BH** and super-spinning sources from the viewpoint of stationary observes. The regions outlined here play a distinct role in the collapse processes with possible spin oscillations and different behaviors for weak, very weak, and strong naked singularities. As the spin increases, the frequencies of **NSs** observes move to lower values, widening the throat. This trend, however, changes with the spin, enlightening some special thresholds.

This analysis shows firstly the importance of the limiting frequency $\omega_0 = M/a$, determining the main properties of both frequencies $\omega_\pm$ and the radii $r_s^\pm$; it is also relevant in relation to ZAMOs dynamics in **NS** geometries. In this way, we may see ω_0 as an extension of the frequency ω_h at the horizon for **BH** solutions – Fig. 4. In the **NS** regime, all the curves $r_s^\pm$ converge to the same "focal point" $r = 0$, regardless of the type of naked singularity, but as ω_h is the limiting frequency at the **BH** horizon, each source is characterized by only one $\omega_0 \neq 0$ frequency. The greater is the spin, the lower is the frequency $\omega_\pm$ at fixed radius, and particularly in the neighborhood of the singularity ring, according to the limiting value ω_0. The frequency range at fixed r/M narrows for higher dimensionless **NS** spin a/M. This feature distinguishes between strong, weak and very weak naked singularities. From Fig. 6 it is clear also that the throat of the light-surfaces $r_s^\pm$, in the plane $r - \omega$, for different spins a/M closes for $a \approx M$, which is a spin transition region that includes the extreme Kerr solution. This region has been enlarged in Fig. 6-bottom. Figures 9 and 10 show from a different perspective the transition between the **BH** region, gray region in Fig. 6, and the **NS** region for different spins. Any spin oscillation in that region generates a tunnel in the light-surface.[13] The transition region is around $\omega_\pm \approx 1/2$,

---

[13] Since any simulation of stellar collapse returns to the **BH** regime, there must be some (retroactive) mechanism that closes the observer tunnel, as even light does not run away in the forbidden region at $r < M$. Moreover, hypothetical super-luminary matter would violate the bonding of the tunnel wall.

which is a special value related to the spin $a = 2M$ of strong naked singularities – see Figs. 3 and 2. In this region, as in the neighborhood of the ring singularity ($r = 0$), the orbital range reaches relatively small values.[14] This shows the existence of limitations for a spin transition in the parameter region of very weak naked singularities, pointed out also in [52–55,76].

On the other hand, in the strong **NSs** regimes, a spin threshold emerges at $a = 2M$ and $a = M$ (see Figs. 3, 4, 6). In Fig. 13, we analyze the properties at the static limit r_ε^+. The maximum value of $\mathscr{E}_-/\mathscr{L}_-$ is then reached in the ergoregion of the **NSII** class.[15] Around $a = a_3$ the throat width becomes more or less constant. The situation is different for $a > a_3$ and $a > 2M$ and then for a_4, where the frequencies range narrows, and near $r = r_\varepsilon^+$ becomes restricted to a small range of a few mass units in the limit of large spin a/M. In strong and very strong **NSs**, the wide region is inaccessible for stationary observers, whereas it is accessible in the **BH** case. This significantly separates strong and weak **NSs**, and distinguish them from the **BH** case. Interestingly, the saddle point around $r = M$, which narrows the throat of frequencies even in the case of **NS** geometries for $a \in]M, a_\sigma[$, could perhaps be viewed as a trace of the presence of r_+, which is absent for $a > M$. For $a = a_\sigma$, where the saddle point disappears, the shape of the $r_s^\pm$ tube is different. This, on the other hand, would suggest that the existence of the flex in the case of very weak **NSs** would prevent a further increasing of the spin. This does not hold for a transition to stronger **NSs**, $a \geq a_\sigma$, where no saddle point is present – Fig. 8-bottom. Obviously, the consequences of the hypothetical transition processes should also take into account the transient phase times. Very weak naked singularities show a "rippled-structure" in the frequency profiles of ω with respect to r/M and a/M, as appears in Figs. 2, 6, 9, and 10. The significance of this structure is still to be fully investigated, but it may be seen perhaps as a fingerprint-remnant of the **BH** horizon. This may open an interesting perspective for the study of **NS** geometries.

An interesting application of our results would be related to the characterization of the optical phenomena in the Kerr naked singularity and black hole geometries, such as the **BH** raytracing and the determination of the **BH** silhouette (shadow). The light escape cones are a key element for such phenomena. Light escape cones of local observers (intended as sources) determine the portion of radiation emitted by a source that could escape to infinity and the one which is trapped. This is related to the study of the radial motion of photons because the boundary of the escape cones is given by directional angles associated to unstable spherical photon orbits. Light escape cones can be identified in locally non-rotating frames, in frames associated to circular geodesic motion and in radially free-falling observers [42,117–120]. We want to point out, however, that light escape cones do not define the properties of the light-cone causal structure, and are not directly related to stationary observers; they rather depend on the photon orbits. A thoroughout analysis of the photon circular motion in the region of the ergoregion can be found in [2]. In Figs. 1, 3, 4 and 12, we show the photon orbit r_γ and the limiting frequencies crossing this radius; this enlightens the relation with the frequency ω_n. We consider there in more detail the relation between the quantities ω_Z ω_*, the constants of motion $\mathscr{L}$ and $\mathscr{E}$ and the effective potential, briefly addressed also in Sect. 4.

In general, we see that it is possible to detect black holes and naked singularities by analyzing the physical properties (orbital radius and frequency) of stationary observers and ZAMOs. Moreover, the main physical properties (mass and angular momentum) of the spinning gravitational source can be determined by measuring the parameters of stationary observers. This is certainly important for astrophysical purposes since the detection and analysis of compact astrophysical objects is one of the most important issues of modern relativistic astrophysics. In addition, the results presented in this work are relevant especially for investigating non-isolated singularities, the energy extraction processes, according to Penrose mechanism, and the gravitational collapse processes which lead to the formation of black holes.

---

[14] It is worth to mention that predicted quantum effects close to the singularities could play a major role in this region. However, we recall that the extreme limit $a = M$ in this model is never faced, as we continue to see the spacetime for all **NSs** using a Boyer–Lindquist frame. It is well known that approaching the horizon at $a = M$, the radial coordinate velocity appears as never penetrating the black hole, spiraling as t goes to infinity. This is the consequence of a coordinate singularity which can be avoided by using Kerr coordinates or Eddington-Finkelstein coordinates.

[15] The throat depth in the region would lead to an immediate change of the observers properties and it is reasonable to ask if this may imply an activation instead of a "positive feedback" phenomenon. We recall that in this scenario, we are not considering a change of symmetries which would have an essential role. Then it is important to emphasize that in these hypothetical spin transitions, the external boundary of the ergoregion remains unchanged, but not the frequency at the static limit.

References

1. R.M. Wald, *General Relativity* (The University of Chicago Press, Chicago, 1984)
2. D. Pugliese, H. Quevedo, Eur. Phys. J. C **75**(5), 234 (2015)
3. J.D. Bekenstein, Phys. Rev. D **7**, 2333 (1973)
4. R.M. Wald, Living Rev. Relativ. **4**(1), 6 (2001)
5. T.M. Fiola, J. Preskill, A. Strominger, S.P. Trivedi, Phys. Rev. D **50**, 3987 (1994)
6. H. Nikolic, Phys. Lett. B **678**, 218 (2009)
7. K. Bradler, C. Adami, JHEP **1405**, 095 (2014)
8. L. Susskind, Sci. Am. **276**(4), 52–57 (1997)
9. S.W. Hawking, Commun. Math. Phys. 43, 199 (1975). [Erratum - ibidem 46, 206 (1976)]
10. S.W. Hawing, Mon. Not. R. Astron. Soc. **152**, 75–78 (1971)
11. R. Penrose, Revista del Nuovo Cimento (1969)
12. J.D. Bekenstein, Phys. Rev. D **12**, 3077 (1975)
13. R. Penrose, R.M. Floyd, Science **229**, 177–179 (1971)
14. F. Gray, S. Schuster, A. Van Brunt, M. Visser, Class. Quantum Gravity **33**(11), 115003 (2016)
15. M. Bejger, T. Piran, M. Abramowicz, F. Hakanson, Phys. Rev. Lett. **109**, 121101 (2012)
16. Z. Stuchlik, P. Slany, G. Torok, M.A. Abramowicz, Phys. Rev. D **71**, 024037 (2005)
17. D.L. Meier, *Black Hole Astrophysics The Engine Paradigm* (Springer, Berlin, 2012)
18. V.P. Frolov, A. Zelnikov, *Introduction to Black Hole Physics*, vol. 488 (Oxford University Press, Oxford, 2011)
19. J. Gariel, G. Marcilhacy, N.O. Santos, Astrophys. J. **774**, 109 (2013)
20. R. Znajek, Nature **262**, 270 (1976)
21. A.R. Prasanna, R.K. Varma, Pramana **8**(3), 229 (1977)
22. A.R. Prasanna, C.V. Vishveshwara, Pramana **11**, 359 (1978)
23. A.N. Aliev, N. Özdemir, Mon. Not. R. Astron. Soc. **336**, 241 (2002)
24. G. Preti, Class. Quantum Gravity **21**, 3433 (2004)
25. P. Bakala, E. Šrámková, Z. Stuchlík, G. Török, Class. Quantum Gravity **27**, 045001 (2010)
26. V.P. Frolov, A.A. Shoom, Phys. Rev. D **82**, 084034 (2010)
27. T. Igata, T. Harada, M. Kimura, Phys. Rev. D **85**, 104028 (2012)
28. R. Shiose, M. Kimura, T. Chiba, Phys. Rev. D **90**, 124016 (2014)
29. S. Hussain, I. Hussain, M. Jamil, Eur. Phys. J. C **74**(12), 3210 (2014)
30. G. Pei, S. Nampalliwar, C. Bambi, M.J. Middleton, Eur. Phys. J. C **76**(10), 534 (2016)
31. S.S. Komissarov, J. Korean Phys. Soc. **54**, 2503 (2009)
32. J.-P. Lasota, E. Gourgoulhon, M. Abramowicz, A. Tchekhovskoy, R. Narayan, Phys. Rev. D **89**(2), 024041 (2014)
33. Z. Stuchlik, J. Kovar, Class. Quantum Gravity **23**, 3935 (2006)
34. Z. Stuchlik, D. Pugliese, J. Schee, H. Kucáková, Eur. Phys. J. C **75**(9), 451 (2015)
35. A. Kotrlová, G. Török, E. Sramková, Z. Stuchlík, A&A **572**, A79 (2014)
36. K. Boshkayev, E. Gasperín, A.C. Gutiérrez-Piñeres, H. Quevedo, S. Toktarbay, Phys. Rev. D **93**, 024024 (2015)
37. M. Kolos, Z. Stuchlík, Phys. Rev. D **88**, 065004 (2013)
38. J. Schee, Z. Stuchlik, JCAP **1304**, 005 (2013)
39. G. Torok, Z. Stuchlik, Astron. Astrophys. **437**, 775 (2005)
40. Z. Stuchlik, Bull. Astron. Inst. Czech **32**(2), 68–72 (1981)
41. Z. Stuchlík, S. Hledík, K. Truparová, Class. Quantum Gravity **28**(15), 155017 (2011)
42. Z. Stuchlik, J. Schee, Class. Quantum Gravity **27**, 215017 (2010)
43. M. Patil, P.S. Joshi, Class. Quantum Gravity **28**, 235012 (2011)
44. Z. Stuchlik, J. Schee, Class. Quantum Gravity **29**, 065002 (2012)
45. Z. Stuchlik, J. Schee, Class. Quantum Gravity **30**, 075012 (2013)
46. K.I. Nakao, P.S. Joshi, J.Q. Guo, P. Kocherlakota, H. Tagoshi, T. Harada, M. Patil, A. Krolak, arXiv:1707.07242 [gr-qc]
47. M.J. Lake, B. Carr, JHEP **1511**, 105 (2015)
48. B.J. Carr, arXiv:1703.08655 [gr-qc]
49. B.J. Carr, J. Mureika, P. Nicolini, JHEP **1507**, 052 (2015)
50. B.J. Carr, Springer Proc. Phys. **170**, 159 (2016)
51. Y. Prok et al. [CLAS Collaboration], Phys. Lett. B **672**, 12 (2009)
52. D. Pugliese, H. Quevedo, R. Ruffini, Eur. Phys. J. C **77**(4), 206 (2017)
53. D. Pugliese, H. Quevedo, R. Ruffini, Phys. Rev. D **83**, 104052 (2011)
54. D. Pugliese, H. Quevedo, R. Ruffini, Phys. Rev. D **88**, 024042 (2013)
55. D. Pugliese, H. Quevedo, R. Ruffini, Phys. Rev. D **84**, 044030 (2011)
56. R. Goswami, P.S. Joshi, P. Singh, Phys. Rev. Lett. **96**, 031302 (2006)
57. C. Vaz, L. Witten, Phys. Lett. B **442**, 90 (1998)
58. H. Iguchi, T. Harada, K.i Nakao, Prog. Theor. Phys. **101**, 1235 (1999)
59. H. Iguchi, K.i Nakao, T. Harada, Phys. Rev. D **57**, 7262 (1998)
60. H. Iguchi, T. Harada, K.I. Nakao, Prog. Theor. Phys. **103**, 53 (2000)
61. S.L. Shapiro, S.A. Teukolsky, Phys. Rev. Lett. **66**, 994 (1991)
62. T.A. Apostolatos, K.S. Thorne, Phys. Rev. D **46**, 2435 (1992)
63. T. Jacobson, T.P. Sotiriou, Phys. Rev. Lett. **103**, 141101 (2009)
64. T. Jacobson, T.P. Sotiriou, J. Phys. Conf. Ser. **222**, 012041 (2010)
65. E. Barausse, V. Cardoso, G. Khanna, Phys. Rev. Lett. **105**, 261102 (2010)
66. B. Giacomazzo, L. Rezzolla, N. Stergioulas, Phys. Rev. D **84**, 024022 (2011)
67. V. Cardoso, P. Pani, M. Cadoni, M. Cavaglia, Phys. Rev. D **77**, 124044 (2008)
68. N. Comins, B.F. Schutz, Proc. R. Soc. A **364**(1717), 211–226 (1978)
69. A. Helou, I. Musco, J.C. Miller, arXiv:1601.05109 [gr-qc]
70. R.M. Wald, V. Iyer, Phys. Rev. D **44**, 3719 (1991)
71. P.S. Joshi, *Gravitational Collapse and Spacetime Singularities* (Cambridge Monographs on Mathematical Physics, New York, 2007)
72. B.P. Abbott et al. (LIGO Scientific Collaboration and Virgo Collaboration), Phys. Rev. Lett. **116**, 061102 (2016)
73. B.P. Abbott et al. [LIGO Scientific and Virgo Collaborations], Phys. Rev. Lett. **119**(16), 161101 (2017)
74. B.P. Abbott et al. [LIGO Scientific and Virgo and Fermi-GBM and INTEGRAL Collaborations], Astrophys. J. **848**(2), L13 (2017)
75. M. Blaschke, Z. Stuchlík, Phys. Rev. D **94**(8), 086006 (2016)
76. D. Pugliese, H. Quevedo, R. Ruffini, Phys. Rev. D **83**, 024021 (2011)
77. D.B. Malament, J. Math. Phys. **18**, 1399 (1977)
78. S.W. Hawking, A.R. King, P.J. McCarthy, J. Math. Phys. **17**, 174 (1976)
79. R.P. Geroch, J. Math. Phys. **8**, 782 (1967)
80. F. de Felice, A&A **34**, 15 (1974)
81. F. de Felice, Nature **273**, 429–431 (1978)
82. Z. Stuchlík, J. Schee, Int. J. Mod. Phys. D **24**, 1550020 (2015)
83. J. Schee, Z. Stuchlik, JCAP **1506**, 048 (2015)
84. J. Gariel, N.O. Santos, J. Silk, Phys. Rev. D **90**, 063505 (2014)
85. N. Pelavas, N. Neary, K. Lake, Class. Quantum Gravity **18**, 1319 (2001)
86. C. Herdeiro, E. Radu, Phys. Rev. D **89**, 124018 (2014)
87. Z. Stuchlik, Bull. Astron. Inst. Czech **31**, 129 (1980)
88. S. Gao, Y. Zhang, Phys. Rev. D **87**(4), 044028 (2013)
89. Z. Stuchlík, M. Blaschke, J. Schee, Phys. Rev. D **96**(10), 104050 (2017)
90. M.H.P.M. van Putten, Prog. Theor. Phys. **127**(2), 331–354 (2012)

91. C.F. Gammie, S.L. Shapiro, J.C. McKinney, Astrophys. J. **602**, 312 (2004)
92. P. Abolmasov, Mon. Not. R. Astron. Soc. **432**, 761–768 (2013)
93. M. Kesden, Phys. Rev. D **83**, 104011 (2011)
94. R.M. Wald, Ann. Phys. **82**, 548 (1974)
95. P. Pradhan, P. Majumdar, Eur. Phys. J. C **73**(6), 2470 (2013)
96. D. Pugliese, G. Montani, Phys. Rev. D **91**(8), 083011 (2015)
97. D. Pugliese, Z. Stuchlik, Astrophys. J. Suppl. **221**, 25 (2015)
98. D. Pugliese, Z. Stuchlik, Astrophys. J. Suppl. **229**(2), 40 (2017)
99. D. Pugliese, Z. Stuchlik, Astrophys. J. Suppl. **223**(2), 27 (2016)
100. D. Pugliese, Z. Stuchlik, JHEAp **17**, 1 (2018)
101. Z. Li, C. Bambi, Phys. Rev. D **87**, 124022 (2013)
102. J. Biéak, Z. Stuchlík, V. Balek, Bull. Astron. Inst. Czech **40**(2), 65–92 (1989)
103. V. Balek, J. Bicak, Z. Stuchlik, Bull. Astron. Inst. Czech **40**(3), 133–165 (1989)
104. J. Kovar, O. Kopacek, V. Karas, Z. Stuchlik, Class. Quantum Gravity **27**, 135006 (2010)
105. S.W. Hawking, G.F.R. Ellis, *The Large Scale Structure of Space–Time* (Cambridge University Press, Cambridge, 1973)
106. C. Chakraborty, M. Patil, P. Kocherlakota, S. Bhattacharyya, P.S. Joshi, A. Krolak, Phys. Rev. D **95**(8), 084024 (2017)
107. A.V. Frolov, V.P. Frolov, Phys. Rev. D **90**(12), 124010 (2014)
108. J.B. Griffiths, J. Podolský, *Exact Space–Times in Einstein's General Relativity* (Cambridge University Press, Cambridge, 2009)
109. L.D. Landau, E.M. Lifshitz, *The Classical Theory of Fields* (Pergamon Press, Oxford, 1980)
110. E. Poisson, *A Relativist's Toolkit: The Mathematics of Black-Hole Mechanics*, 1st edn. (Cambridge University Press, Cambridge, 2004)
111. M.R.R. Good, Y.C. Ong, Phys. Rev. D **91**(4), 044031 (2015)
112. P .T. Chrusciel, J. Lopes Costa, Living Rev. Relativ. **15**, 7 (2012)
113. B. Carter, arXiv:gr-qc/9712038
114. R.M. Wald, Class. Quantum Gravity **16**, A177 (1999)
115. S. Chandrasekhar, *The Mathematical Theory of Black Holes* (Oxford University Press, Oxford, 1983)
116. C.W. Misner, K.S. Thorne, J.A. Wheeler, *Gravitation* (Freeman, San Francisco, 1973)
117. J. Schee, Z. Stuchlik, J. Juran, Proceedings of RAGtime 6/7: Workshops on black holes and neutron stars, Opava, 16-18/18-20 September, 2004/2005
118. J. Schee, Z. Stuchlik, Int. J. Mod. Phys. D **18**, 983 (2009)
119. R. Takahashi, M. Takahashi, A&A **513**(A77), 7 (2010)
120. J. Schee, Z. Stuchlik, Gen. Relativ. Gravit. **41**, 1795 (2009)